REPORT DOCUMENTATION PAGE

Form Approved
OMB No. 0704-0188 2

1. AGENCY USE ONLY *(Leave blank)*	2. REPORT DATE	3. REPORT TYPE AND DATES COVERED
	July 1998	Final (1 Jul 96 - 30 Jun 98)

4. TITLE AND SUBTITLE
Improved Breast Cancer Detection Using a Novel In Situ Method to Visualize Clonality

5. FUNDING NUMBERS
DAMD17-96-1-6120

6. AUTHOR(S)
John Zebala, Ph.D

7. PERFORMING ORGANIZATION NAME(S) AND ADDRESS(ES)
Children's Hospital and Medical Center
Seattle WA 98105

8. PERFORMING ORGANIZATION REPORT NUMBER

9. SPONSORING/MONITORING AGENCY NAME(S) AND ADDRESS(ES)
Commander
U.S. Army Medical Research and Materiel Command
Fort Detrick, Frederick, Maryland 21702-5012

10. SPONSORING/MONITORING AGENCY REPORT NUMBER

19981118 053

11. SUPPLEMENTARY NOTES

12a. DISTRIBUTION / AVAILABILITY STATEMENT

Approved for public release; distribution unlimited

12b. DISTRIBUTION CODE

13. ABSTRACT *(Maximum 200*

We report the successful development of a sensitive clonality assay. The assay is based on a novel method we have developed termed "biolithography" which applies photolithography, a process known in the semiconductor industry, to biologic material. Biolithography uses diazoquinone photoresist and targeted light irradiation to isolate DNA from selected cell populations under direct microscopic visualization with 100% specificity and sensitivity at the limit of PCR. Using biolithography, we have detected clonality from as few as 20 neoplastic cells. We have also discovered abnormal demethylation of the X chromosome at the human androgen receptor and PGK genes in several cases of breast carcinoma. Microsatellite analysis of markers closely linked to genes involved in X chromosome inactivation has identified loss of heterozygosity which correlates with demethylation. Consistent with the stepwise model of tumor progression, demethylation of both X chromosomes may reflect abnormal activation of X chromosomes. These studies demonstrate the utility of biolithography to discern subtle molecular changes in solid tumors which may exist in only microscopic regions. Efforts have also been made to increase the throughput of biolithography for potential translation to the clinical laboratory. Investigations of photoresists with ultra-high photosensitivity and laser driven systems are encouraging, and suggest the possibility of high-throughput systems. Biolithography may thus provide new opportunities for molecular diagnostics of solid tumors.

14. SUBJECT TERMS
Old: Breat Cancer, FISH, clonality, ligase, cytopathology, X chromosome, DNA methylation///New: Photolithography, photoresist, X inactivation, demethylation, XIST, microsatellite, biolithography

15. NUMBER OF PAGES
55

16. PRICE CODE

17. SECURITY CLASSIFICATION OF REPORT	18. SECURITY CLASSIFICATION OF THIS PAGE	19. SECURITY CLASSIFICATION OF ABSTRACT	20. LIMITATION OF ABSTRACT
Unclassified	Unclassified	Unclassified	Unlimited

AD_______________

Grant Number DAMD17-96-1-6120

TITLE: Improved Breast Cancer Detection Using a Novel In Situ Method to Visualize Clonality

PRINCIPAL INVESTIGATOR: John Zebala, Ph.D.

CONTRACTING ORGANIZATION: Children's Hospital and Medical Center
Seattle, Washington 98105

REPORT DATE: July 1998

TYPE OF REPORT: Final

PREPARED FOR: U.S. Army Medical Research and Materiel Command
Fort Detrick, Maryland 21702-5012

DISTRIBUTION STATEMENT: Approved for public release; distribution unlimited

The views, opinions and/or findings contained in this report are those of the author(s) and should not be construed as an official Department of the Army position, policy or decision unless so designated by other documentation.

FOREWORD

Opinions, interpretations, conclusions and recommendations are those of the author and are not necessarily endorsed by the U.S. Army.

____ Where copyrighted material is quoted, permission has been obtained to use such material.

____ Where material from documents designated for limited distribution is quoted, permission has been obtained to use the material.

✓ Citations of commercial organizations and trade names in this report do not constitute an official Department of Army endorsement or approval of the products or services of these organizations.

____ In conducting research using animals, the investigator(s) adhered to the "Guide for the Care and Use of Laboratory Animals," prepared by the Committee on Care and use of Laboratory Animals of the Institute of Laboratory Resources, national Research Council (NIH Publication No. 86-23, Revised 1985).

✓ For the protection of human subjects, the investigator(s) adhered to policies of applicable Federal Law 45 CFR 46.

____ In conducting research utilizing recombinant DNA technology, the investigator(s) adhered to current guidelines promulgated by the National Institutes of Health.

____ In the conduct of research utilizing recombinant DNA, the investigator(s) adhered to the NIH Guidelines for Research Involving Recombinant DNA Molecules.

____ In the conduct of research involving hazardous organisms, the investigator(s) adhered to the CDC-NIH Guide for Biosafety in Microbiological and Biomedical Laboratories.

John [illegible] 7/30/98

PI - Signature Date

FINAL REPORT
Grant # DAMD17-96-1-6120
PI: John A. Zebala, M.D., Ph.D.

TABLE OF CONTENTS

INTRODUCTION

Subject

Breast carcinoma is one of the major causes of death in women, affecting about 1 in 10 North American women [1]. The risk of mortality from breast cancer can be reduced with early detection [2]. Mammography is the most sensitive technique currently available for detecting early disease. A mammogram, however, is not a diagnostic test for cancer but only a screening test. A diagnosis requires biopsy and examination by a pathologist. In many centers, the biopsy is a surgical biopsy with total costs measured in thousands of dollars. Of women who undergo surgical biopsy for an abnormal mammogram, only 30% have cancer while 70% are benign [3]. Surgical consultations and biopsies for benign disease represent the major induced cost of screening with $2 billion spent annually [4]. As mammographic sensitivity improves, the number of biopsies for benign disease will only increase as will the cost of identifying each cancer. Surgical biopsies also carry a certain amount of risk, are anxiety provoking, painful, leave the woman with some degree of scarring, and may contribute to noncompliance with screening mammography programs in general [5].

A less expensive alternative to surgical biopsy is fine-needle aspiration biopsy (FNAB), which involves aspirating cells from a mass with a very thin needle while the patient is awake. The procedure requires as few as 20 minutes to arrive at a diagnosis, is extremely well tolerated, and costs 1/20 th that of surgical biopsy. The premise of FNAB is that a diagnosis may be made by examining the cytology of cells.

Although FNAB has been in use for over a century, an inherent weakness is that aspiration destroys some of the architectural information normally seen in routine tissue sections. Roughly 20% of breast smears are equivocal or insufficient, resulting in surgical biopsy for definitive diagnosis with no cost savings [6, 7]. Particularly difficult is the distinction of precancerous and potentially curable lesions (ductal carcinoma in situ, atypical ductal hyperplasia) from the atypical changes often seen in benign disease [8]. Current recommendations suggest that as an alternative to costly surgery, benign conditions may be clinically monitored [9]. Diagnostically challenging FNAB cases will only become more prevalent as mammography advances. In the past, these shortcomings have led to an under-utilization of FNAB in favor of the more accurate, but considerably more expensive surgical biopsy. Economic changes in health care, however, have significantly increased the demand and expectations of FNAB to accurately detect the small, early and curable lesions while keeping total cost to a minimum.

Purpose/Hypothesis

To meet these needs, we proposed to improve the diagnostic accuracy of breast FNAB by developing a novel *in situ* fluorescent assay for clonality based on X chromosome inactivation (i.e. methylation). It was our hypothesis that combining an *in situ* assay for clonality with standard morphologic examination would increase the

diagnostic accuracy of FNAB for breast cancer, because the hallmark of neoplasia is the clonal proliferation of cells.

Brief Summary of Work

We report here the successful development of a sensitive clonality assay with capabilities beyond the *in situ* fluorescent assay originally proposed. The assay is based on a novel method we have developed termed "biolithography" which applies photolithography, a process known in the semiconductor industry, to biologic material. A major obstacle to developing molecular diagnostics for solid tumors is the need to isolate cell populations of interest from the vast majority of native, normal cells. Homogenized tumor samples reflect the average content of all cell types present, precluding the analysis of clonality and tumor cell-specific alterations including loss of heterozygosity (LOH) and homozygous deletions.

Biolithography overcomes these limitations by utilizing a diazoquinone based photoresist and targeted light irradiation to isolate DNA from selected cell populations under direct microscopic visualization with high specificity and subcellular resolution. Using biolithography, we have detected clonality from as few as 20 neoplastic cells. We have also discovered abnormal demethylation of the X chromosome at the human androgen receptor and PGK1 genes in DNA isolated from the pre-cancerous (DCIS) and invasive components of several cases of breast carcinoma.

Although still very preliminary, microsatellite analysis of several markers closely linked to genes involved in X chromosome inactivation has identified LOH near the XIST gene which correlates with demethylation. Consistent with the stepwise model of tumor progression, demethylation of both X chromosomes may reflect an abnormal reactivation of maternal and paternal X chromosomes.

Neither X chromosome demethylation or LOH could be detected using conventional microdissection methods, demonstrating the utility of biolithography to discern subtle molecular changes in solid tumors which may exist in only microscopic regions. Biolithography has the potential for laboratory automation and provides a source of material for all DNA based tests including chip based genetic panel testing and comparative genomic hybridization.

Finally, efforts have been made to increase the throughput of biolithography by exploring alternative photoresists with ultra-high photosensitivity, and laser driven systems which simplify the process steps of biolithography. Although not presently as evolved as the diazoquinone photoresists, encouraging results have been obtained from these studies suggesting the feasibility of high-throughput biolithography.

This work has been presented in detail at a meeting of the Academy of Clinical Laboratory Physicians and Scientists in Minneapolis, Minnesota on June 5-7, 1997. Manuscripts describing this work are in preparation.

Background

A major obstacle to developing molecular diagnostics for solid tumors is the need to isolate cell populations of interest from the vast majority of native, normal cells. This reflects a general difficulty in assigning position-composition relationships in a multicellular organism when one cell type interferes with the detection of another. For example, homogenized tumor samples reflect the average content of all cell types present, precluding the analysis of tumor cell-specific deletions including LOH and homozygous deletions because of the presence of normal cells containing a complete set of genetic material.

Clonal proliferations may be detected using an *in vitro* PCR assay to detect the methylation status of the human androgen receptor gene on the X chromosome [10]. However, this assay is also limited by the need to separate neoplastic from normal cells [11]. Failure to do so results in erroneous polyclonal patterns for DCIS and ADH due to contaminating normal cells.

In situ methods detect position-composition relationships by directly contacting biologic material, usually while on a glass slide, with an assay mixture for a particular composition. The assay mixture produces a visible product which co-localizes with the composition it detects, revealing position-composition relationships by visual inspection. Although we previously proposed an *in situ* fluorescent method to obviate the need to separate neoplastic from normal cells, such methods also have limitations including the types of compositions that can be detected, the sensitivity and specificity of detection, the number of assays that can be performed on the same biologic material, the need for human interpretation, and the difficulty in automating process steps.

In contrast, *in vitro* methods detect one or more compositions with an assay whose products homogenously distribute in the assay mixture. The average content of all compositions present in the sample are detected rather than specific position-composition relationships. Despite this drawback, advantages of *in vitro* methods include a wide variety of detectable compositions, outstanding sensitivity and specificity, multiple and often simultaneous assays on the same material, and the ease by which process and interpretation steps may be automated. However, if material is isolated in a highly regioselective fashion, position-composition relationships can be evaluated by *in vitro* methods by correlating the position of isolated material with its composition.

Previous investigators have described methods that claim to provide position-composition relationships using *in vitro* methods. Several physical dissection methods have been described including gross dissection of frozen tissue blocks to enrich for specific cell populations [12, 13], and "touch preparations" of frozen tissue specimens [14]. These methods do not visualize regions of interest microscopically. Selection capabilities are therefore crude, resulting in significant sample contamination. Microdissection using a dissecting microscope has been described providing for better

isolation of selected material [11, 15, 16]. However, microdissection suffers from being labor intensive and impractical for routine clinical use.

Others have generated genetically stable cell expansions, free of infiltrating nonneoplastic cells by growing xenografts in athymic *nude* mice [17, 18]. However, this method results in xenograft contamination with up to 50% murine cells, requires weeks for growth, cannot be automated, requires living cells, applies only to autonomously growing cells, and may artifactually alter the composition of cells through the introduction of mutations in the xenograft.

An ultraviolet light-mediated method has been described which destroys unwanted genetic material except where it has been manually ink-stained with an ink-pen [19]. This method, known as selective ultraviolet radiation fractionation (i.e. SURF), suffers from a very crude resolution dictated by the size of the ink-pen and requires up to 30 minutes of ultraviolet exposure to destroy unwanted material. Biomolecules are also limited to those sensitive to ultraviolet light. Other disadvantages include the need to transfer the material to a tube (either with or without the underlying substrate), the manual application of ink, the difficulty of automating process steps, and a mixture typically containing irradiated material in vast abundance. The latter can contribute to inhibiting sensitive amplification methods such as PCR.

Laser capture microdissection (LCM) is a recently described method that utilizes a transparent thermoplastic film (ethylene vinyl acetate, EVA) to capture cells from glass slides under direct visualization [20]. EVA is applied to the surface of a tissue section placed on a glass slide and irradiated with a carbon dioxide laser using infrared radiation. The laser energy is absorbed by the film which adheres to the underlying selected cells, which are selectively procured when the film is removed. Drawbacks of LCM include less than 100% transfer of cells to the EVA film, a glass surface that must be specially prepared so as to facilitate tissue lift-off, and a ragged border between irradiated and non-irradiated regions (i.e. low contrast). Because the entire EVA film is transferred from the slide surface to a reaction tube, there is the potential for contamination of the non-irradiated EVA with tissue fragments. The latter is a significant disadvantage when sensitive amplification methods for detection are employed (e.g. PCR). Also, cumbersome automation and robotics are required in the transfer process resulting in a high system cost. Another disadvantage is a resolution limited by the wavelength of the infrared laser (~10 microns) which precludes microdissection of subcellular components.

We report the development of a novel method termed "biolithography" which overcomes these limitations by utilizing photoresist and targeted light irradiation to isolate DNA from selected cell populations under direct microscopic visualization with high specificity and subcellular resolution. Air-dried or paraffin embedded material may be used. Biolithography detects position-composition relationships using the advantages of *in vitro* methods with reduced potential for contamination compared to LCM. Although currently manually performed, the process has the potential to be automated.

Using biolithography, we have detected clonality from as few as 20 neoplastic cells. We have also discovered abnormal demethylation of the X chromosome at the human androgen receptor and PGK1 genes in DNA isolated from the pre-cancerous (DCIS) and invasive components of several cases of breast carcinoma. Microsatellite analysis of several markers closely linked to genes involved in X chromosome inactivation has identified LOH which correlates with demethylation. Consistent with the stepwise model of tumor progression, demethylation of both X chromosomes may reflect an abnormal reactivation of maternal and paternal X chromosomes. Neither X chromosome demethylation or LOH could be detected using conventional microdissection methods, demonstrating the utility of biolithography to discern subtle molecular changes in solid tumors.

EXPERIMENTAL METHODS

Applying Biologic Material to Glass Slides

Glass slides were coated with either male lymphocytes, breast cancer cell lines, sections of normal breast tissue, or sections of breast cancer tissue as follows: Breast cancer cell lines HTB131 and HTB129 (American Type Culture Collection, Rockville, MD) were maintained as monolayer cultures in 75 cm^2 tissue culture flasks (Corning, New York) in RPMI 1640 medium (Gibco BRL, Grand Island, NY) supplemented with 6 mM L-glutamine, 10 μg/ml human insulin and 10% fetal calf serum, buffered with 14 mM sodium bicarbonate, 20 mM Hepes, and 20 μg/ml gentamicin. Cells were washed with 1x phosphate buffered saline (PBS) followed by incubation with 0.25% trypsin at 37^{o}C for 5 min. Cells were harvested from the flask, washed with 1x PBS, and resuspended in 1x PBS at a concentration range of 1×10^6 cells/ml to 9×10^6 cells/ml. Alternatively, peripheral male lymphocytes were obtained from peripheral blood using Ficoll-Paque® PLUS (Pharmacia, Uppsala, Sweden) according to the manufacturer's instructions, and resuspended in 1x PBS at a concentration range of 1×10^6 cells/ml to 9×10^6 cells/ml. Approximately 20 μl were taken from either the suspensions of breast cancer cells or male lymphocytes, and applied to a 1 cm^2 area of a standard, or positively-charged glass slide and allowed to air-dry. Positively-charged glass slides treated with aminopropyltrimethoxysilane were commercially obtained (Curtin-Matheson Scientific, Inc., Houston, TX). Occasionally, equal volumes (about 10 μl each) of breast cancer cells and male lymphocytes were intentionally applied to the same area of the slide. The cells were then hydrated with graded alcohols and subsequently stained with hematoxylin and eosin according to standard procedures. After staining with eosin, the cells were dehydrated in graded alcohols and allowed to air-dry.

Normal breast and breast cancer specimens from females were fixed in 10% buffered formalin and paraffin embedded according to standard tissue processing methods. From the paraffin embedded specimens, 5 μm thick sections were prepared, and placed on positively-charged glass slides. The sections were deparaffinized with two, 10 minute washes with xylene. The sections were then hydrated with graded alcohols and

subsequently stained with hematoxylin and eosin according to standard procedures. After staining with eosin, the sections were dehydrated in graded alcohols and allowed to air-dry.

Isolation of DNA From Irradiated Areas

The reactor cavity was filled with 100 μl of 100 mM Tris-HCl buffer at pH 8.0 containing 10 mM EDTA, and allowed to incubate for 1 hour. The reactor cavity was then rinsed twice with 100 μl of 100 mM Tris-HCl buffer at pH 8.0. This was followed by overnight incubation at 37°C with 100 μl of "extraction solution" containing 50 mM Tris-HCl (pH 8.0), 1 mM EDTA, and 0.4 mg/ml to 1.0 mg/ml of proteinase K. After overnight incubation, the extraction solution was withdrawn from the reactor cavity and transferred to a 0.7 ml polypropylene tube. The extraction solution was then incubated at 80°C for 30 minutes to heat denature the proteinase K while retaining DNA in the duplex form. The tube was then subjected to a brief centrifugation for 30 seconds to bring down any condensate. Aliquots of the extraction solution were used in subsequent methods.

Specificity and Sensitivity

All the extraction solution, or 100 ng of DNA isolated by conventional methods, was amplified in a total volume of 130 μl containing 1 μM each of primers AR-F and AR-R as follows:

AR-F: 5′ TCCAGAATCTGTTCCAGAGCGTGC 3′
AR-R: 5′ GCTGTGAAGGTTGCTGTTCCTCAT 3′

in combination with 250 μM dNTPs (Boehringer Mannheim, Indianapolis, IN), 3.0 U *Taq* polymerase (Boehringer Mannheim, Indianapolis, IN), 5.0 μCi alpha-^{32}P-dCTP (New England Nuclear, Boston, MA), 1.5 mM $MgCl_2$, 50 mM KCl, and 50 mM Tris-HCl (pH 8.3). Amplification was performed using an automated thermocycler (Perkin-Elmer, Branchburg, NJ) for 40 cycles (cycle = 60s @ 94°C, 75s @ 61°C, 75s @ 72°C), followed by a 72°C soak for 10 min. Reactions without added DNA were included as negative controls (not shown).

A 4 μl aliquot of each sample was combined with an equal volume of loading buffer containing 98% deionized formamide, 10 mM EDTA, 0.2% xylene cyanol, and 0.2% bromophenol blue followed by denaturation at 94°C for 2 min. Amplification products were separated by electrophoresis for 2-3 hours at 65 Watts constant power in a 5% polyacrylamide gel containing 7 M urea, 100 mM Tris borate (pH 8.9), and 1 mM EDTA. The gel was dried onto 3 mm paper (Whatman) and autoradiographed overnight at -70°C on XAR-5 film (Kodak) with an intensifying screen. Product lengths were determined by comparison with an external size standard or by direct DNA sequencing (not shown).

Site-Specific Cleavage of DNA: Methylation Patterns and Clonality

From 50 to 500 total cells were irradiated per 5 μm paraffin section. Extraction solution was prepared from each as described above. For each extraction solution, a reaction without ("-RE") and with ("+RE") restriction enzymes was prepared consisting of 20 μl of extraction solution in a total volume of 26 μl containing 56 mM Tris-HCl (pH 8.3), 2.6 mM $MgCl_2$, and 10 units each of *Cfo*I and *Hpa*II in the "+RE" reaction. All reactions were incubated for 5 hours at 37^{o}C, followed by heat inactivation of the restriction enzymes at 65^{o}C for 10 min.

1. Detection of clonality using the androgen receptor (AR) gene

The entire "-RE" and "+RE" reactions were amplified in a total volume of 33 μl containing 1 μM AR-F and AR-R primers, 250 μM dNTPs (Boehringer Mannheim, Indianapolis, IN), 2.5 U *Taq* polymerase (Boehringer Mannheim, Indianapolis, IN), 4.0 μCi alpha-^{32}P-dCTP (New England Nuclear, Boston, MA), 1.5 mM $MgCl_2$, 50 mM KCl, and 95 mM Tris-HCl (pH 8.3). Amplification was performed using an automated thermocycler (Perkin-Elmer, Branchburg, NJ) for 40 cycles (cycle = 60s @ 94^{o}C, 75s @ 61^{o}C, 75s @ 72^{o}C), followed by a 72^{o}C soak for 10 min. Reactions without added DNA were included as negative controls (not shown).

A 4 μl aliquot of each sample was combined with an equal volume of loading buffer containing 98% deionized formamide, 10 mM EDTA, 0.2% xylene cyanol, and 0.2% bromophenol blue followed by denaturation at 94^{o}C for 2 min. Amplification products were separated by electrophoresis for 2-3 hours at 65 Watts constant power in a 5% polyacrylamide gel containing 7 M urea, 100 mM Tris borate (pH 8.9), and 1 mM EDTA. Amplification products from each extraction solution were loaded on the gel as "-RE" and "+RE" pairs. The gel was dried onto 3 mm paper (Whatman) and autoradiographed overnight at -70^{o}C on XAR-5 film (Kodak) with an intensifying screen.

2. Dection of clonality using the PGK gene

The entire "-RE" and "+RE" reactions were amplified in a total volume of 69 μl containing 1 μM PGK-1a and PGK-1b primers (see below), 250 μM dNTPs (Boehringer Mannheim, Indianapolis, IN), 2.5 U *Taq* polymerase (Boehringer Mannheim, Indianapolis, IN), 1.5 mM $MgCl_2$, 50 mM KCl, and 95 mM Tris-HCl (pH 8.3). Amplification was performed using an automated thermocycler (Perkin-Elmer, Branchburg, NJ) for 40 cycles (cycle = 75s @ 94^{o}C, 120s @ 58^{o}C, 120s @ 72^{o}C), followed by a 72^{o}C soak for 10 min.

An 8 μl aliquot of each reaction above was then amplified in a total volume of 80 μl containing 0.5 μM PGK-2a and PGK-2b primers (see below), 250 μM dNTPs (Boehringer Mannheim, Indianapolis, IN), 8.0 U *Taq* polymerase (Boehringer Mannheim,

Indianapolis, IN), 4.0 μCi alpha-^{32}P-dCTP (New England Nuclear, Boston, MA), 1.5 mM $MgCl_2$, 50 mM KCl, and 95 mM Tris-HCl (pH 8.3). Amplification was performed using an automated thermocycler (Perkin-Elmer, Branchburg, NJ) for 40 cycles (cycle = 90s @ 94^{o}C, 120s @ 58^{o}C, 120s @ 72^{o}C), followed by a 72^{o}C soak for 10 min. Following amplification, a 7 μl aliquot of each reaction was digested with 10 units BstXI in a total volume of 35 μl containing approximately 50 mM Tris-HCl (pH 8.3), 10 mM $MgCl_2$, and 100 mM NaCl. All reactions were incubated for 5 hours at 55^{o}C, followed by heat inactivation of the restriction enzymes at 70^{o}C for 10 min.

Samples (20 μl) were separated as "-RE" and "+RE" pairs by electrophoresis for 2-3 hours at 65 Watts constant power in a 3.5% polyacrylamide gel containing 100 mM Tris borate (pH 8.9), and 1 mM EDTA. The gel was dried onto 3 mm paper (Whatman) and autoradiographed overnight on XAR-5 film (Kodak).

The following nested primers were used in the PGK PCR reactions:

PGK-1a: 5′ CTGTTCCTGCCCGCGCGGTGTTCCGCATTC 3′
PGK-1b: 5′ ACGCCTGTTACGTAAGCTCTGCAGGCCTCC 3′
PGK-2a: 5′ AGCTGGACGTTAAAGGGAAGCGGGTCGTTA 3′
PGK-2b: 5′ TACTCCTGAAGTTAAATCAACATCCTCTTG 3′

Detection of Lost Genetic Material: Microsatellite Analysis

Five μm thick paraffin-embedded sections were applied to substrates as described above. Specific regions of interest were located and irradiated using well recognized morphologic characteristics. From 50 to 500 total cells were irradiated per substrate. Extraction solution was prepared from each irradiated substrate as described above, and categorized as either normal ("N"), DCIS ("D"), or cancer ("C").

For each microsatellite marker, two PCR assays were prepared using "N" and "C" extraction solutions. Occasionally, a PCR assay was also prepared using "D" extraction solution. Primers flanking each microsatellite marker were commercially obtained (MapPairs™, Research Genetics, Huntsville, AL). For each PCR assay, a 5 μl aliquot of extraction solution was amplified in a total reaction volume of 15 μl containing 1 μM primers, 250 μM dNTPs (Boehringer Mannheim, Indianapolis, IN), 1.2 U *Taq* polymerase (Boehringer Mannheim, Indianapolis, IN), 3.0 μCi alpha-^{32}P-dCTP (New England Nuclear, Boston, MA), 1.5 mM $MgCl_2$, 50 mM KCl, and 50 mM Tris-HCl (pH 8.3). Amplification was performed using an automated thermocycler (Perkin-Elmer, Branchburg, NJ) for 40 cycles (cycle = 60s @ 94^{o}C, 60s @ 55^{o}C, 60s @ 72^{o}C), followed by a 72^{o}C soak for 10 min.

A 4 μl aliquot of each sample was combined with an equal volume of loading buffer containing 98% deionized formamide, 10 mM EDTA, 0.2% xylene cyanol, and 0.2% bromophenol blue followed by denaturation at 94^{o}C for 2 min. Amplification products were separated by electrophoresis for 2-3 hours at 65 Watts constant power in a 5%

polyacrylamide gel containing 7 M urea, 100 mM Tris borate (pH 8.9), and 1 mM EDTA. Amplification products for each microsatellite marker were loaded on the gel as "N", "C" or "N", "D", "C" groups. The gel was dried onto 3 mm paper (Whatman) and autoradiographed overnight at -70°C on XAR-5 film (Kodak) with an intensifying screen.

PROCEDURES

Applying and Photopatterning the Photoresist

While working in a laminar flow hood illuminated by cool-white fluorescent lights shielded with Gold Shields [Imtec Products Inc., Sunnyvale, CA], AZ® 1512 positive photoresist [Hoechst Celanese™, Somerville, NJ] was applied using a Pasteur pipette without dilution to the surface of biologic material on a glass slide prepared as described above. The excess was allowed to drain onto a paper towel by positioning the slide vertically. The slide was then placed on a flat surface for approximately 3 minutes at room temperature to partially evaporate the solvent, followed by soft-baking on a metal heating block at a temperature of from 90°C to 100°C for 1 to 2 minutes or in an oven at a temperature of from 90°C to 100°C for 15-30 minutes to completely evaporate the solvent. Partial evaporation of the solvent at room temperature prior to soft-baking was discovered to be critical for reproducibly achieving a glassy photoresist layer upon complete evaporation. The evaporated layer of photoresist was 5 μm to 10 μm thick as determined by profilometry.

The slide was then transferred to the irradiation-targeting device illustrated in FIG. 8. Light from long bandpass filter **214** transilluminated the substrate in area **228**. Biologic material in area **228** was visualized through the translucent photoresist **30** using objective **208**, microscope **206**, and ocular optics **224**. Specific regions of interest were located using x/y translation table **202** according to particular morphologic characteristics.

A region of interest was then positioned so that it encompassed area **226**. If the region of interest was relatively large, area **226** was enlarged using iris diaphragm **218**. Conversely, if the region of interest was relatively small, area **226** was decreased using iris diaphragm **218**. With a region of interest appropriately in position, mechanical shutter **216** was opened allowing light from excitation filter **205** to epi-illuminate substrate **20** and photoresist **30** in area **226**. Area **226** was visualized as a red fluorescent circle during epi-illumination. The temporal progress of the photochemical reaction was visualized by the formation of microscopic bubbles within photoresist **30** in area **226**. The photochemical reaction was typically complete in 3 to 5 seconds with a 10x objective and a 50 Watt mercury lamp, and complete in less time with 20x and 40x objectives. The substrate was successively repositioned with shutter **216** open and iris diaphragm **218** appropriately re-adjusted until an entire region of interest was epi-illuminated. The substrate was then translated to a discontinuous region of interest

with the shutter closed, and the above process repeated until all regions of interest were irradiated.

Developing the Photoresist and Applying the Reactor System

With the photoresist appropriately photopatterned as described above, the entire substrate was immersed in AZ® 351 developer diluted six-fold with distilled water [Hoechst Celanese™, Somerville, NJ]. The photoresist in irradiated regions was completely dissolved after about 30 seconds in developer. The temporal progress of dissolution was visually monitored by the formation of red dye from irradiated regions during the development process. The dye is thought to form by the reaction of indene carboxylic acid (IV) with unreacted diazoquinone. After an additional 30 seconds in developer, the biologic material in irradiated regions lost both hematoxylin and eosin stains, appearing clear and translucent to the naked eye. After a total of 60 seconds in developer, the entire substrate was rinsed with distilled water three times, and allowed to air-dry. Subsequent steps were carried out under illumination with standard cool-white fluorescent lights. A reactor system was formed with a nylon cylinder [Eagle Hardware, Seattle, WA] mated to the photoresist surface with silicone adhesive (Dow-Corning, Midland, MI) as depicted in FIG. 7.

RESULTS AND DISCUSSION

Address to the Statement of Work

The Statement of Work is reproduced below for convenience. Each task is briefly addressed sequentially in the larger sized type. The work accomplished is described in detail in later sections.

Statement of Work

Technical Objectives 1 and 2: Cell lines as a model system and initial attempts to detect clonality using noncircular and circular approaches

Task 1: Months 1-2: The allelic status of cell lines are defined using the PCR assay.

Completed.

Task 2: Months 2-6: Preliminary noncircular and circular approaches are applied to cell lines to determine feasibility.

Noncircular and circular approaches failed to yield adequate signal above background. These were abandoned in favor of biolithography which proved successful for detecting clonality from as few as 20 cells and having other broad capabilities as well. Subsequent tasks were completed using this method as a substitute for the originally proposed *in situ* fluorescent approaches.

Technical Objective 3: Clonality assays are optimized.

Task 1: Months 6-12: Using the cell lines, experiments are performed to optimize noncircular and circular approaches with respect to temperature, ligase concentration, probe concentration and washing stringency.

Optimization of biolithography successfully completed.

Task 2: Months 6-12: Specificity experiments are performed.

Specificity and sensitivity experiments successfully completed using biolithography.

Task 3: Months 12-18: Depending on the success of noncircular and circular approaches, mask-FISH is developed and feasibility tested. The efficiency of antibody masking and antibody removal is evaluated.

Mask-FISH abandoned in favor of biolithography.

Task 4: Months 12-18: Depending on the success of noncircular and circular approaches, the resolution of mask-FISH is determined.

Resolution of biolithography successfully determined.

Technical Objective 4: The hypothesis is tested on surgical specimens

Task 1: Months 12-24: A test set of surgical specimens are collected which consist of normal breast, benign fibroproliferative disease, fibroadenoma, ADH, DCIS, and invasive malignancy. FNAB is performed and a blinded diagnosis is rendered by the cytopathologist.

Completed with caveats (see Recommendations).

Task 2: Months 12-24: Clonality assays are performed on the smears and the pathologist renders a second diagnosis based on the new information. Results are tabulated against the final histologic diagnosis and statistical analysis performed.

Completed with caveats (see Recommendations).

Supplemental Technical Objective 5: Increase the throughput of biolithography to improve the potential for translation from research to clinical utility.

Task 1: Explore photosensitive compositions with enhanced photospeed to increase the rate biolithography may be performed for compatibility with clinical laboratory use.

Completed.

Task 2: Test alternative photosensitive compositions and methods with fewer process steps to simplify the method of biolithography.

Completed.

In short, the research has successfully addressed the Statement of Work. Superior solutions have been provided where initially proposed strategies were subsequently abandoned.

The Method of Biolithography

Biolithography provides a method for exposing discrete regions of biologic material in a highly precise and specific manner utilizing light irradiation as depicted in FIG. 1 through FIG. 7. FIG. 1 illustrates a glass substrate **20** shown in cross-section. Surface **22** of the substrate is coated with a layer of linker molecules **24** selected based upon their ability to promote adhesion of biologic material **26**, **27**, and **28**. Although the biologic material may adequately adhere to the glass without a layer of linker molecules, in the following experiments adhesion was promoted with aminopropyltriethoxysilane as the linker molecule. The biologic material is typically formalin fixed tissue sections or air-dried cells stained with hematoxylin and eosin.

As shown in FIG. 2, a positive photoresist **30** is applied with a pipette to the stained biologic material and substrate surface, and allowed to drain by gravity by vertically positioning the substrate. The photoresist solvent is allowed to evaporate leaving a film approximately 5 μm thick as determined by profilometry. Evaporation of the solvent is accelerated by heating at 90^{o}C for 1 minute. The final thickness of the evaporated film may be controlled by altering the percent solids by diluting the photoresist with an organic solvent (e.g. 2-ethoxyethyl acetate, 1-methoxy-2-propyl acetate, or 3-pentanone). A relative decrease in film thickness results in a corresponding decrease in the required irradiation time, resulting in a more rapid irradiation process.

In our hands, the photoresist with the most desirable properties tested thus far is from the class of commercially available diazoquinone containing positive photoresists [see U.S. Pat. Nos. Steinhoff *et al.*, 3,402,044; Moore, 2,797,213; Endermann *et al.*, 3,148,983; Schmidt, 3,046,118; Neugebauer *et al.*, 3,201,239; Sus, 3,046,120; Fritz *et al.*, 3,184,310; Borden, 3,567,453; and Pampaione, 4,550,069]. Positive photoresists allow irradiated regions to be solubilized with dilute, aqueous, alkaline solutions while non-irradiated regions are insoluble. Non-irradiated regions and irradiated regions, however, are both rapidly solubilized by a variety of organic solvents (e.g. acetone).

Positive photoresists generally comprise a non-photoactive phenol-formaldehyde resin in concentration from about 10 to 40 wt% and a photosensitive diazoquinone in concentration from about 10 to 40 wt% in an organic solvent, such as 2-ethoxyethyl acetate or 1-methoxy-2-propyl acetate. Other additives, such as surfactants, may be present in minority fractions to promote planarization of the photoresist. The photolytic response of these photoresists reflect the photochemistry of the photosensitive diazoquinone often also referred to as a diazoketone, diazo-oxide, diazoanhydride, or quinone diazide, a chemical of the general form:

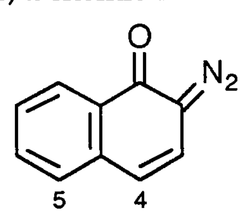

where the most commonly used versions of the general form are substituted at positions 4 or 5 with an -SO_2R group, where R consists of a very large variety of functionalities including sulfonic acid esters and amides of both monomeric and polymeric hydroxy, phenoxy, and amino compounds well described in the patent literature [21]. The primary photochemical behavior of the diazoquinone is the same regardless of the composition of R.

Although the mechanism is not completely understood, absorption of any radiation with wavelengths from about 220 to 450 nm at ambient conditions is thought to raise the diazoquinone (I) to a higher energy state [22]. This higher energy state decomposes very rapidly with loss of nitrogen gas from the diazo group to form an unstable and very reactive keto-carbene (II) as shown:

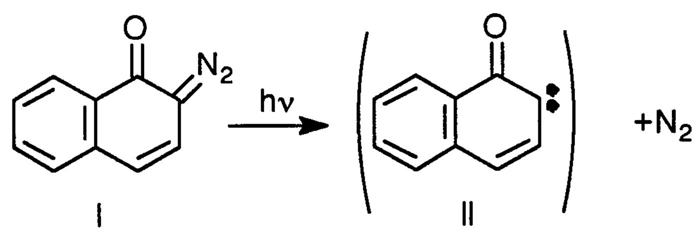

I II

The transient species immediately isomerizes by ring contraction to a more stable intermediate called a ketene (III) as shown:

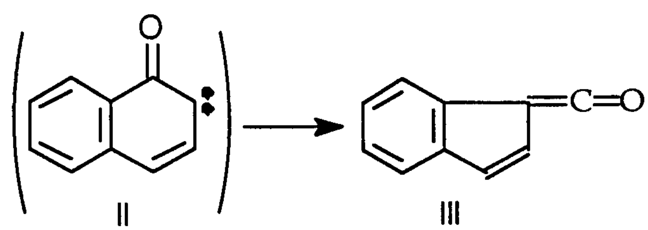

II III

The ketenes themselves are quite reactive and combine readily with many reagents. It is thought that the ketenes combine with trace water to form the indene carboxylic acid (IV) as below:

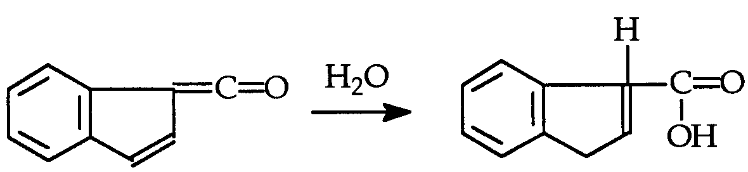

III IV

This sequence of events, which includes the photolytic conversion of an initially insoluble diazoquinone (I) to an acid species (IV) soluble in aqueous alkaline solutions leads to a differential solubility in alkali between irradiated and non-irradiated photoresist.

We hypothesize that the absence of any deleterious effect on the contacted biologic material by the reactive photolytic intermediates may be due to the intramolecular aspect of the photolytic process.

The substrate and biologic material are visualized directly using optical microscopy and trans-illumination with a light **32** of a wavelength greater than 500 nm that does not react with the photoresist (see FIG. **3**). This light is obtained with a long bandpass filter that passes 535-700 nm irradiation.

As shown in FIG. **4**, the photoresist is irradiated with a second light **34** that is reactive to the photoresist. Although these two lights function independently, the first and second lights generally irradiate the surface simultaneously with the second light irradiating a sub-portion of the region irradiated by the first light. In the experiments described below, the photoresist is an AZ® 1500 series positive photoresist [Hoechst Celanese™, Somerville, NJ], irradiated for between 1 and 5 seconds with light **34** from a 50 Watt mercury lamp filtered with an excitation filter that passes about 400-440 nm irradiation. The light is focused with either 10x, 20x or 40x objective lenses providing for a relative increase in Watts/cm^2 of 100x, 400x and 1600x, respectively. The relative increase in Watts/cm^2 results in a corresponding decrease in the required irradiation time.

The process of irradiating the photoresist is repeated with the second light **34** until all regions of interest in the biologic material have been irradiated (see FIG. **5**). The second light is blocked by a manual shutter when the substrate is translated between non-contiguous regions. As shown in FIG. **6**, the process of irradiating all regions of interest is completed, and the entire substrate is contacted with a developing solution resulting in dissolution and removal of photoresist from irradiated regions **36** and **38**. In the experiments described below, the substrate is immersed in AZ® 351 Developer [Hoechst Celanese™, Somerville, NJ] diluted six-fold with water for about 30 to 60 seconds at room temperature. The temporal progress of dissolution is visually monitored by the formation of red dye from irradiated regions during the development process. The dye is thought to form by the reaction of indene carboxylic acid (IV) with unreacted diazoquinone. It has been discovered that the alkaline developer provides the additional advantage of destaining the biologic material of hematoxylin and eosin; an important advantage as stains are inhibitors of certain reactions including PCR.

FIG. **7** schematically illustrates the reactor system **39** which holds an extraction solution thereby allowing extraction of DNA from exposed biologic material **27** and **28**, but not unexposed biologic material **26** since it is blocked by a layer of photoresist. The reactor system includes a body **40** mated to a photoresist surface **44** creating a reaction chamber **42**. The body and a separable cover **46** serve to seal the cavity. The reactor body is cylindrical with interior walls sloping towards the center so as to facilitate working with small volumes.

Purification of DNA is typically performed by the addition of a protease followed by extractions with organic solvents and precipitation with ethanol. However, multiple purification steps increase the probability of losing DNA during the purification of samples obtained by biolithography as they typically contain only few cells (i.e. <1000). Accordingly, a simplified DNA isolation method was devised eliminating organic

solvents and precipitation steps thereby minimizing the probability of losing DNA (see Experimental Methods).

Biolithography provides a method with the important advantage that biologic material does not have to be removed from the glass substrate to a separate reaction vessel as with LCM. In effect, the glass substrate and the reactor system become a "reaction tube". This aspect, and the ability to select regions of interest with light, together provide significant advantages compared to removing biologic material from the glass substrate. These include superior accuracy, sensitivity, purity, resolution, contrast, speed, and simplicity of process automation.

The Irradiation-Targeting Device

FIG. **8** illustrates the irradiation-targeting device for visualizing and irradiating discrete regions of the photoresist using the method as described above. The glass substrate **20**, which has been coated with biologic material and photoresist **30**, is placed on a manually operated x/y translation table **202**. The substrate and x/y translation table are under a microscope **206** which includes one or more objectives **208**. The x/y translation table, microscope and objectives are all members of a Standard Microscope [Carl Zeiss, Thornwood, NY]. The irradiation-targeting device is best understood by considering the visualization and photopatterning subsystems separately, followed by the operation of these subsystems.

1. Visualization

Light from a first lamp **212** is passed consecutively through an iris diaphragm **213**, a long bandpass filter **214**, and a condenser **215** to transilluminate substrate **20** in an area **228**. Lamp **212**, iris diaphragm **213**, and condenser **215** are components of a Standard Microscope equipped with a 100 Watt halogen lamp, model no. 380059-1660 [Carl Zeiss]. The long bandpass filter [model no. A43,386, Edmund Scientific Co., Barrington, NJ] passes 535 nm to 700 nm light from the first lamp. Light from transilluminated area **228** is collected by objective **208** and microscope **206** and directed to a dichromatic beam splitter **207**. The dichromatic beam splitter [model FT460, Carl Zeiss] passes greater than about 470 nm light, reflecting light less than this. Thus, the 535 nm to 700 nm light from first lamp **212** passes through the dichromatic beam splitter, and is directed to a barrier filter **222**. The barrier filter [model LP470, Carl Zeiss] passes greater than about 470 nm light to ocular optics **224** for visualization by a user.

2. Photopatterning

Light from a second lamp **210** is passed consecutively through a lamp condenser **220**, an iris diaphragm **218**, an open mechanical shutter **216**, and an excitation filter **205**. The second lamp, condenser, iris diaphragm, and mechanical shutter are all members of a Vertical Illuminator IV FL fitted with a 50 Watt mercury lamp [Carl Zeiss]. The excitation filter [BP400-440 excitation filter, Carl Zeiss] passes 400 nm to 440 nm light from second lamp **210**. Light passed by excitation filter **205** is directed at dichromatic

beam splitter 207. The dichromatic beam splitter passes greater than 470 nm light, reflecting light less than this. Thus, 400 nm to 440 nm light passed by excitation filter 205 is reflected 90 degrees by dichromatic beam splitter 207. Light from the dichromatic beam splitter is collected by microscope 206 and objective 208 and directed to substrate 20 forming an epi-illuminated area 226 on photoresist 30.

3. Operation

Long bandpass filter 214 functions to provide transillumination of substrate 20 with a wavelength of light that does not react with photoresist 30 in area 228. The photoresist is translucent allowing the user to visualize and locate regions of interest in the biologic material using x/y translation table 202 without concern for causing a reaction in photoresist 30.

Excitation filter 205 functions to provide epi-illumination of substrate 20 with a wavelength of light that reacts with photoresist 30 in area 226. The process of photoresist epi-illumination is benefited by two unique properties of the diazoquinone photoresist. First, epi-illumination of the diazoquinone photoresist results in 510 nm to 560 nm fluorescence in area 226 which is visualized as a red circle within area 228. This allows the user to identify the size and borders of the region being photopatterned concurrently with visualization of area 228. Second, the photochemical reaction produces nitrogen gas which may be visualized as microscopic bubbles within photoresist layer 30 in area 226. The formation of microscopic bubbles is a convenient visual indicator of the temporal progress of the photochemical reaction within photoresist layer 30.

Although regions 226 and 228 may be of any size or shape, region 228 is typically a circle that occupies an objective's full field-of-view. In contrast, region 226 is typically a circle of variable size. The size of region 226 is adjusted using iris diaphragm 218 according to the size and shape of the desired photopattern. For example, the photopattern size may encompass thousands of cells, a single cell, or a subcellular component. The substrate is exposed to light from second lamp 210 when manual shutter 216 is open. However, the manual shutter is closed when the substrate is translated between discontinuous photopatterned regions. Thus, the process of visualization and photopatterning is achieved by manipulating x/y translation stage 202, iris diaphragm 218, and manual shutter 218 until all regions of interest in the biologic material have been irradiated. Virtually any shape can be photopatterned using this process and a multitude of overlapping circular regions 226 of varying size.

Specificity and Sensitivity

Specificity was measured by determining how selectively DNA was extracted from an equal mixture of male lymphocytes and HTB129 cells (a breast cancer cell line). The male lymphocytes and HTB129 cells contain 18 and 23 CAG repeats in the human androgen receptor gene, respectively. This feature allowed the composition of extracted DNA to be identified by performing PCR with primers flanking the CAG repeat.

Three separate glass substrates were prepared containing the 50:50 mixture of male lymphocytes and HTB129 cells. Each substrate was irradiated at either male lymphocytes, HTB129 cells, or male lymphocytes and HTB129 cells with 50 to 100 total cells irradiated per substrate. Examples of single exposed male lymphocytes using this process are depicted in the scanning electron micrographs in FIG. 9 (debris around lymphocytes are platelets). Note the superior resolution and contrast with smooth borders that are sharp and steep between irradiated and unirradiated regions.

DNA was extracted from each irradiated substrate and PCR amplified using primers which flank the CAG repeat. DNA isolated from pure populations of male lymphocytes or HTB129 cells using conventional methods served as positive controls.

Bands from the autoradiographed gel are depicted in FIG. 10. The product containing the greater number of trinucleotide repeats has a slower mobility because it is larger. Doublet bands are produced for each allele because each strand of the denatured duplex has a slightly different mobility. Lanes 4 and 5 represent the positive controls. As expected, PCR of male lymphocyte DNA results in the $(CAG)_{18}$ product (lane 4), and PCR of HTB129 DNA results in the $(CAG)_{23}$ product (lane 5). Lanes 1 through 3 represent each of the three substrates prepared as described above. The substrate irradiated at both male lymphocytes and HTB129 cells results in both $(CAG)_{18}$ and $(CAG)_{23}$ products (lane 1). However, substrates irradiated at either male lymphocytes (lane 2) or HTB129 cells (lane 3) yield amplification products that are 100% specific to the irradiated cells with irradiation of the male lymphocytes resulting in the $(CAG)_{18}$ product (lane 2), and irradiation of the HTB129 cells resulting in the $(CAG)_{23}$ product. There is no evidence of amplification products from unirradiated cells even upon prolonged exposure of the gel to film for one week.

The outstanding specificity demonstrated in FIG. 10 is corroborated by directly examining the substrate as shown in FIG. 11. The left panel shows irradiated regions of destained, male lymphocytes prior to the addition of extraction solution containing proteinase K. The right panel shows that the irradiated cells are selectively procured after the addition of extraction solution, and that cells in unirradiated regions are unaltered. Furthermore, this is apparent even in cells as close as 1 μm to an irradiated region.

Sensitivity was demonstrated by applying male lymphocytes to five glass substrates and isolating DNA from decreasing numbers of irradiated cells per glass substrate. Irradiation of 50, 20, 5, 1 and 0 male lymphocytes were performed separately on each of the five substrates. DNA was extracted from each irradiated substrate, PCR amplified, electrophoresed, and autoradiographed according to the above Experimental Methods, except that the gel was autoradiographed for 5 days. The autoradiograph is depicted in FIG. 12. Amplification product is visualized from as few as 5 irradiated lymphocytes. This demonstrates that the method has exquisite sensitivity equivalent to the limit of PCR.

Site-Specific Cleavage of DNA: Methylation Patterns and Clonality

The following experiments demonstrate the capability of biolithography to detect methylated DNA compositions and clonality from minute regions of normal and cancerous tissues using site-specific DNA cleavage. Results from these studies also reveal the approximate "patch" size of methylation in normal female tissues, as well as novel patterns of abnormal methylation in some cases of breast carcinoma and its precursor lesions.

As previously noted by Lyon, only one of two X chromosomes is active in a somatic female cell with the inactive X chromosome methylated at CG sequences [23]. Inactivation is a random event occurring early in embryogenesis resulting in inactivation of either the maternal or paternal X chromosome. Thus, normal female tissue is a mosaic, consisting of clusters of maternally inactivated cells adjacent to clusters of paternally inactivated cells. The size of a cluster, or "patch" is not completely known.

The somatic mutation theory of carcinogenesis states that a malignant neoplasm represents the clonal expansion of a single mutated somatic cell that acquired a selective growth advantage over its normal counterparts [24, 25]. Such clones will all maintain the same X inactivation pattern as the patch from which they arose. Breast carcinoma, as well as the precancerous lesions of ductal carcinoma *in situ* (DCIS) and atypical ductal hyperplasia (ADH) are clonal proliferations bearing the same X inactivation pattern [11, 26].

The following experiments detect clonality indirectly by assaying methylation patterns of the X chromosome using the human androgen receptor gene as a surrogate marker of methylation [10]. With reference to FIG. 13, a female somatic cell methylates either the maternal or paternal androgen receptor gene (located at Xq13). The trinucleotide repeat in the coding region of the androgen receptor gene consists of 20 alleles ranging from 11 to 31 repeats with 92% heterozygosity. PCR with primers flanking the polymorphic repeat will amplify both alleles. This may be seen as two bands after electrophoresis (see "-RE" lanes in FIG. 13). However, if the DNA is digested with methylation-sensitive restriction enzymes prior to PCR, the unmethylated template is cleaved and amplification occurs only from the methylated allele (see "+RE" lanes in FIG. 13).

Normal tissue generally results in amplification of both maternal and paternal alleles because half of the patches contain a methylated maternal allele and half contain a methylated paternal allele (i.e. a polyclonal pattern). This is seen as two bands after gel electrophoresis ("+RE" lanes in FIG. 13 superimposed). Previous investigators have not established methylation patterns from single patches, or determined the relative size of patches. A pure malignant population will produce only one of two bands because the same methylation pattern is maintained in all malignant cells.

To detect methylated DNA compositions and clonality, 5 μm thick paraffin embedded sections were applied to substrates. Specific regions of interest were located and irradiated using morphologic characteristics well recognized by pathologists. Regions of interest included breast epithelium, squamous epithelium, smooth muscle, lymphoid tissue, vasculature, DCIS, and nests of primary breast cancer. Normal tissues found in cancer such a vasculature, stroma and inflammatory cells were carefully avoided so as to obtain DNA from cancer cells only. From 50 to 500 total cells were irradiated per substrate. DNA was prepared resulting in about 100 μl of extraction solution from each substrate. Two 20 μl aliquots were removed from each extraction solution to generate a reaction without ("-RE") and with ("+RE") restriction enzymes. The "+RE" reaction contained the methylation sensitive restriction enzymes *Cfo*I and *Hpa*II. The "-RE" and "+RE" reactions were further manipulated as described in the Experimental Methods.

Using the resolution capabilities of biolithography, the methylation patterns of single patches were examined. The results from breast cancer cases 3413 and 2767 are depicted in FIG. 14. Normal tissues were found to have a monoclonal methylation pattern when irradiated in sufficiently small regions encompassing a single patch. For example, the gland epithelium ("EP") and vasculature ("VASC") in case 3413, and the lymph node ("LN") and squamous epithelium ("SQ") in case 2767 all had a monoclonal methylation pattern. However, when the irradiated region was expanded to encompass more than one patch, a polyclonal pattern was found as in the smooth muscle ("SM") in case 2767.

The relationship of irradiation area and methylation pattern from a preliminary study of six cases is summarized in the graph in the bottom half of Table I with black rectangles representing clonal and white rectangles representing polyclonal populations. From this data it is seen that a typical patch is probably on the order of a fraction of a millimeter rather than being of microscopic dimensions as has been previously assumed. This is corroborated by studies from Tsai *et al.* who identified clonal populations in a number of normal microdissected breast ducts of similar dimensions as those irradiated in this study [27]. The implications of these findings to the diagnostic potential of clonality testing may be found in the Recommendations section below.

Two separate irradiated regions of DCIS in case 3413 were found to have the same allele methylated as expected based on the somatic mutation theory of carcinogenesis. The cancer in case 2767 illustrates loss of genetic material which often occurs in the stepwise progression of cancer (compare the "-" and "+" lanes). In this case, the androgen receptor gene was deleted from the inactive X chromosome.

Surprisingly, in some cases of DCIS and breast cancer it was discovered that neither X chromosome was methylated. With reference to FIG. 15, two alleles were amplified from the cancer in case 1639 (lane 1), but upon restriction enzyme digestion, neither allele was amplified (lane 2). To test for the possibility of a PCR inhibitor, additional DNA was added to the heat inactivated restriction enzyme digest prior to PCR

amplification. No PCR inhibitor was detected as both alleles amplified (lane 3). To test more generally for the presence of diffusible molecules or degradative enzymes which could have inhibited either the restriction enzymes or the thermostable polymerase, DNA from the cancer in case 3413 was added as an internal control. The cancer in case 3413 contained a monoclonal methylation pattern (compare lanes 6 and 7). Equal amounts of DNA from cases 1639 and 3413 were combined, and in the absence of restriction enzymes all four alleles amplified (lane 8). In the presence of restriction enzymes, only the allele from case 3413 (i.e. the positive internal control) amplified (lane 9). This demonstrates that there were no trans-acting inhibitors of either the restriction enzymes or the thermostable polymerase. The lack of allele amplification from case 1639 upon restriction enzyme digestion is therefore due to absent methylation rather than a diffusible factor.

Absent X chromosome methylation in case 1639 was not detected using a microdissection technique [11, 16, 20]. Two microdissection efforts each resulted in a polyclonal methylation pattern (lanes 4 and 5). Polyclonal tissues inter-mixed with cancer cells such as vasculature and lymphocytes were difficult to avoid using microdissection probably accounting for the result.

In another case, the phenomenon of demethylation was spatially examined as depicted in FIG. **16a**. The evolution of demethylation correlated progressively with position within the mass. The DCIS appeared to have started with a monoclonal methylation pattern (B3, B7) followed by demethylation (B5, B8) and eventually deletion of genetic material peripherally (B12). The cancer presumably arose as a subclone of the intermediate, demethylated stage (B10). The progression of these events in a spatially ordered fashion from the precancerous to cancerous stages suggest that demethylation of the X chromosome may be involved in the stepwise progression of breast cancer.

A summary of cases studied to date may be found in table I, where M2 = both alleles methylated, polyclonal; M1 = one allele methylated, clonal; and M0 = no alleles methylated, demethylation. The number in front of the designation reflects the number of samples taken for that particular case. For example, "3M1" indicates that three separate regions of glandular epithelium gave a monoclonal pattern for case 1196. As can be seen, there is a general pattern of demethylation as one moves from normal to cancerous tissue.

The involvement of methylation in carcinogenesis is not unprecedented [for review see Feinberg [28]]. For example, Feinberg and Vogelstein described hypomethylation of the human growth hormone gene and globin genes in colon and lung cancer [29]. Rainier *et al.* have shown relaxation of imprinting of the insulin-like growth factor 2 (IGF2) gene on 11p15 in Wilms' tumor of the kidney [30]. Relaxation of imprinting results in overexpression of IGF2 in Wilms' tumors, and it has been suggested that this mitogenic peptide may enhance the growth of these tumors through an autocrine mechanism. Patients with the Beckwith-Wiedemann syndrome, an overgrowth condition associated with Wilms' tumor and several other malignancies, have

abnormalities of IGF2 imprinting in a variety of normal cells. It has been suggested that the abnormal IGF2 imprinting in this syndrome leads to a constitutive cancer diathesis with an increased incidence of Wilms' tumor. A substantial fraction of lung, colon and breast cancers also show loss of IGF2 imprinting.

By analogy, methylation of genes on the inactive X chromosome represents a gross imprinting event. Widespread X chromosome demethylation would therefore have a major impact on the cell, potentially affecting the dosage of hundreds of genes. However, it is tenuous to use the androgen receptor gene as the sole indicator of X chromosome demethylation since it is only a surrogate marker of X chromosome inactivation and represents only a small fraction of the entire X chromosome. In order to more accurately define the extent of X chromosome demethylation, we examined the methylation status of another polymorphic locus (i.e. PGK1) significantly distant from the androgen receptor gene.

Methylation of PGK1 and androgen receptor genes were determined similarly, except that PGK1 paternal and maternal alleles were distinguished by detecting a polymorphism at a *Bst*XI site (see Experimental Methods for details). As depicted in FIG. **16a**, neither X chromosome was methylated at the androgen receptor in the cancer from case 1196. However, the monoclonal pattern of the DCIS (B3, B7) was the same as the monoclonal pattern of the adjacent normal breast epithelium (data not shown).

The methylation status of the adjacent normal breast epithelium was examined using PGK1. As seen in FIG. **16b**, the slower migrating band represents the methylated allele (compare -RE and +RE lanes). Examination of the cancer with PGK1 revealed loss of methylation at this allele, and a deletion of PGK1 from the other allele (faster migrating band, compare -RE lanes from cancer and normal epithelium). The rationale for assigning demethylation to the slower migrating band of the cancer is based on the knowledge that the monoclonal methylation patterns of the normal breast epithelium and the DCIS (B3, B7) are identical (see above), and that the cancer arose from the DCIS. Thus, two loci (i.e. PGK1 and AR) separated by 12.6 MB demonstrate demethylation. The implications of this finding are that demethylation may extend over megabases of DNA and possibly could involve the entire X chromosome.

Although methylation is generally associated with inactivation of genes on the X chromosome, Panning and Jaenisch have shown that hypomethylation activates XIST expression and silences X-linked genes [31]. Thus, the net effect of demethylation on gene expression in breast cancer is uncertain. Our provisional model for how demethylation may be involved in breast carcinogenesis is shown in FIG. **21**. It is similar to models proposed for the role of relaxed imprinting on carcinogenesis [29]. Either activation or inactivation of genes on the X chromosomes could be consistent with carcinogenesis. While inactivation would likely lead to unregulated growth if it affected essential tumor suppressers, activation might promote growth by way of excessive expression of growth factors.

These studies demonstrate significant advantages of biolithography over other methods. Biolithography provides highly accurate position-composition relationships using *in vitro* methods. Superior resolution, contrast, and selection allowed detection of methylation patterns in single mosaic patches, clonality of tumors, and the discovery of a potentially novel mechanism of carcinogenesis involving demethylation of the X chromosome. It is likely that understanding other position-composition relationships will further our understanding of carcinogenesis in a variety of tumors.

Detection of Lost Genetic Material: Microsatellite Analysis

Functional loss of essential tumor suppressors is a key mechanism in the stepwise progression of cancer. Loss usually occurs by deletion of at least one tumor suppressor gene together with kilobases and often megabases of adjacent DNA. Deletion of the tumor suppressor gene may be indirectly detected using a linked microsatellite marker. Marker heterozygosity occurs when maternal and paternal alleles have a different number of repeats. Loss of heterozygosity (LOH) is seen when a tumor suppressor gene is deleted together with the adjacent microsatellite marker, and the cell is left with a single microsatellite allele. Occasionally, a homozygous deletion occurs, leaving no alleles.

An obstacle to identifying LOH is the fact that tumors are heterogeneous, containing tumor cells as well as various normal cells. DNA from homogenized tumor samples reflects the average content of all cell types present in the sample; abnormal and normal. The presence of genetic material from contaminating normal cells often obscures LOH. As such, prior studies recognize the need to isolate tumor cells away from normal cells before a microsatellite analysis is applied. Biolithography satisfies this need, providing for the detection of LOH directly from solid tumors.

Although there is an analogy between imprinting and X inactivation, each is maintained by different molecular systems. The system responsible for establishing and maintaining X inactivation has been extensively defined over recent years [32, 33]. We hypothesized that the phenomenon of X chromosome demethylation was likely due to loss of one or more genes in the system normally responsible for maintaining X inactivation. In order to potentially identify the molecular basis for demethylation, we asked whether we could detect deletion of markers closely linked to genes known to be involved in the X inactivation process. These genes included the DNA methyltransferase (DNMT), the methyl CG binding protein 2 (MECP2), the X inactive specific transcript (XIST), and a cytogenetic region involved in choosing which X chromosome is inactivated (Xq27.3). Very preliminary results suggest that deletions around the XIST gene correlate with demethylation.

A microsatellite analysis was conducted using markers linked to the above genes or loci and LOH was detected in several paraffin-embedded breast cancers. From 50 to 500 total cells were irradiated per substrate. Extraction solution was prepared from each irradiated substrate as described in the Experimental Methods, and categorized as either normal ("N"), DCIS ("D"), or cancer ("C"). LOH was present when one of the

heterozygous amplification products in the "N" lane was missing in the "D" or "C" lanes. Abnormal priming of the polymerase accounts for minor amplification products as previously documented by others.

The results from breast cancer case 1639 are depicted in FIG. 17. There was no evidence of LOH except at the DXS8092 marker. Compare "N" and "C" lanes in the last panel of FIG. 17. Using biolithography, LOH at the DXS8092 marker was repeated twice with identical results (see FIG. 18, center two lanes). LOH at DXS8092 was not detected using a microdissection technique presumably because of contaminating normal cells (last lane).

As shown in FIG. 20, the DXS8092 marker is 5' of the XIST gene within a 300 kb region previously shown by Migeon and colleagues using ring X chromosomes to be required for initiation of X inactivation [34]. The DXS8092 marker is flanked by two heterozygous markers (DXS8037 and DXS1221) defining the maximum possible deleted region to be 70 kb. Although more studies are required, it is interesting to speculate the LOH at DXS8092 and demethylation are related.

Given the location of DXS8092, it is possible that this deletion causes demethylation by disrupting the normal function of the X Inactivation Center (XIC). The X Inactivation Center (XIC) is necessary in *cis* for counting the number of active X chromosomes in a cell, and for initiating and spreading inactivation through the entire length of the X chromosome [34]. The XIST gene lies within the XIC region and is thought to encode a structural RNA that complexes in *cis* with the X chromosome. In contrast to all other X-linked genes, XIST is expressed exclusively from the inactive X chromosome. XIST spreads bidirectionally from the XIC, inactivating the entire length of the X chromosome [31]. Methylation is thought to be an additional and redundant mechanism insuring maintenance of the inactive state.

Penny *et al.* have recently shown that chromosomes without functional XIST are incapable of undergoing inactivation, but are still able to be counted [35]. Thus, the spreading sequence and the counting sequence are physically separable elements within the XIC. Brown and Willard have show that the inactive state is stably maintained after the loss of the entire XIST region on the human X chromosome, which suggests that although XIST is required for initiation and propagation, it is not required for the maintenance of X inactivation [36].

Based on the work of Brown and Willard, disrupting XIST expression would not be expected to result in demethylation. However, the effect of many generation of cell growth as occurs in a solid tumor could lead to an outcome different from that identified by Brown and Willard. Alternatively, demethylation could be consistent with disruption of the counting element. In such a case, the active X containing the deleted counting element might become "invisible" to the counting mechanism, resulting in inappropriate demethylation and activation of the inactive X chromosome.

Conversely, case 2767 show LOH at MECP2 and Xq27.3 as depicted in FIG. 19, but does not demonstrate demethylation, suggesting that these loci are not involved. In total, over 300 microsatellite analyses have been performed using biolithography as summarized in Table II, where N = noninformative, H = heterozygous, and LOH = loss of heterozygosity. These studies illustrate the capability of biolithography to detect deleted DNA compositions from minute regions of cancer or its precursors embedded in normal tissue.

High-Throughput Biolithography

Although biolithography is effectively performed with diazoquinone photoresist, throughput is limited by relatively slow photospeed (80 mJ/cm^2) and wet development. These factors restrict routine use of diazoquinone photoresist to research applications. In order to translate biolithography to direct patient care, we investigated alternative lithographic systems with enhanced photospeed and/or dry development.

a. Photoresists with Enhanced Photospeed

Several candidate lithographic systems were screened for rapid photospeed and biologic compatibility. The water-soluble photopolymer PVA-SBQ derived from stilbazolium (SBQ) substituted poly(vinyl alcohol) (PVA) was selected for further investigation as a potential diazoquinone substitute [37]. PVA-SBQ is prepared by cyclic acetal formation between 1,3-diol units of PVA and a formylstyrylpyridinium salt:

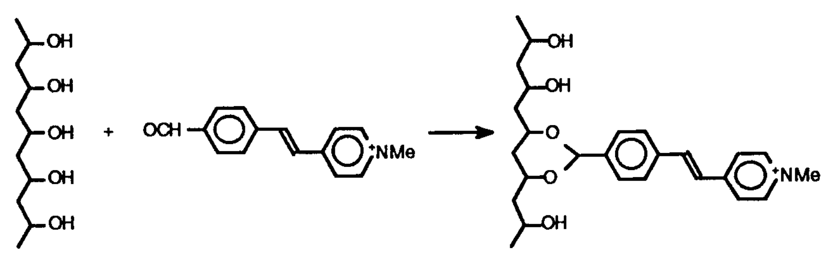

Irradiation of PVA-SBQ with longwave ultraviolet light initiates covalent (2+2) photocycloaddition and formation of a cyclobutane ring between SBQ moieties:

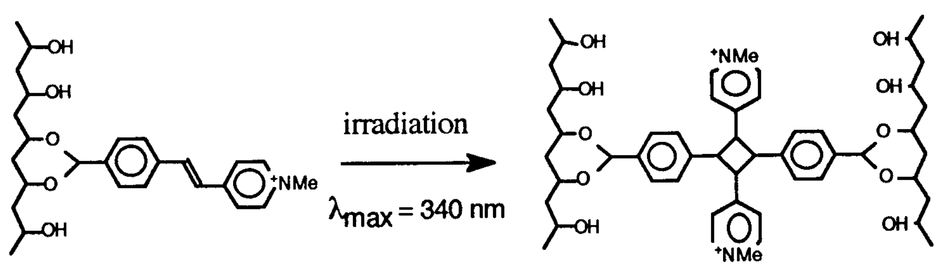

Photopatterned PVA-SBQ is developed in water which removes non-irradiated polymer, resulting in a *negative photoresist* system.

Novel features of PVA-SBQ are its high photosensitivity (1-3 mJ/cm^2), low mol% substitution of PVA with SBQ, and biologic compatibility. These features are the result of a unique property of PVA-SBQ whereby non-covalent dimers of SBQ form in the solid-state. SBQ dimers provide a structural configuration which lead to highly efficient and therefore highly photosensitive crosslinking. Because SBQ units are non-covalently paired before irradiation, an anomalously low mol% substitution of PVA is sufficient for crosslinking and insolubilization. Finally, dimerization results in biologic compatibility because photoreactive species are paired and do not participate with the underlying biologic material.

Preliminary experiments were performed to assess the feasibility of isolating DNA from male lymphocytes using PVA-SBQ as a substitute for diazoquinone photoresist. Glass substrates were prepared containing male lymphocytes. An aqueous mixture of 2% PVA-SBQ (PVA 1 mol% substituted with SBQ) and 0.1% Triton (surfactant; promotes planarization of film) was applied to a slide surface as described above for diazoquinone photoresist (see Procedures section). Because PVA-SBQ is a negative photoresist, irradiation was performed over the entire film except in areas selected for DNA removal. The entire substrate was then exposed to water which resulted in the rapid dissolution and removal of PVA-SBQ from non-irradiated regions.

As anticipated, PVA-SBQ was superior to diazoquinone photoresist in its photosensitivity, requiring ~20-fold less irradiation than diazoquinone photoresist. However, difficulties arose after prolonged contact between extraction solution and developed film. There was marked swelling of the film which resulted in dehiscence from the substrate and loss of physical separation between irradiated and non-irradiated regions.

Swelling is due to water interpenetrating the crosslinked network, driven by the same forces that dissolve non-irradiated regions. It is exacerbated when the density of covalent crosslinks is low. With only 1 mol% of PVA hydroxyls substituted with SBQ, photo-crosslinked PVA-SBQ retains the same high affinity for aqueous solutions as unmodified PVA.

Attempts were made to increase the mechanical strength of PVA-SBQ films by blending polymer additives known to decrease swelling, and by increasing the density of covalent crosslinks in the film through ion-assisted crosslinking. Polymer additives included high molecular weight PVA (70,000 g/mole) and poly(vinyl pyrrolidone) up to an equal weight basis of PVA-SBQ. These additives mitigated swelling, but not to the extent required for the practical application of biolithography.

Ion-assisted crosslinking utilizes borate ions to form di-diol complexes in basic solution that are PVA-specific thereby avoiding any chemical interaction with the underlying cellular material. It was reasoned that the PVA-SBQ film could be mechanically strengthened by the addition of borate ions in the pre-cast PVA-SBQ solution (attempts to crosslink PVA-SBQ films by exposure to borate solution

subsequent to photopatterning were unsuccessful). The mechanism of ion-assisted crosslinking of PVA is not entirely clear, but ^{11}B-n.m.r. data indicates that two diol units of PVA chains react with one borate ion (pK_a of 9.0) to form a crosslink according to the following mechanism [38]:

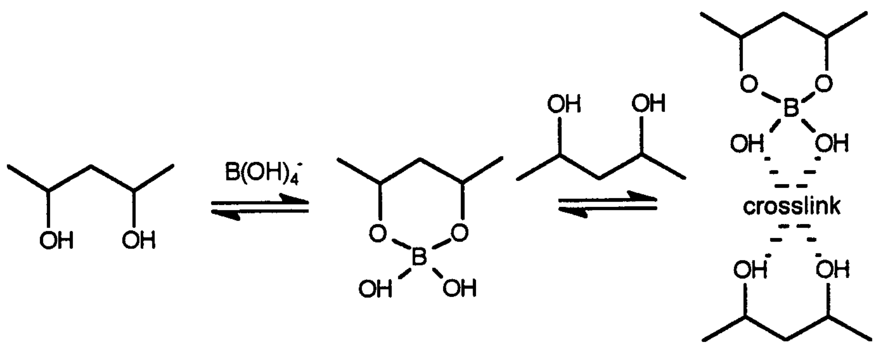

It was hypothesized that pre-cast PVA-SBQ solutions would remain stable below a borate concentration where solvation of polymer chains and electrostatic repulsion of monodiol units dominated (first reaction above). As solvent evaporated from cast films, polymer chains would approximate one another and crosslinking would dominate the final solid-state film. Films could then be photopatterned and developed in slightly acid, aqueous solutions. Conversely, a collapse transition of pre-cast PVA-SBQ solutions would be expected above a certain borate concentration if the polymer-polymer attractive interaction was greater than the repulsive and solvent interactions.

Based on these theoretical assumptions, the optimum concentration of borate ions for pre-cast PVA-SBQ solutions was determined empirically by varying the PVA-SBQ hydroxyl to borate ratio and polymer concentration as shown in the following data table:

	PVA-SBQ (wt%)	Borate (mM)	NaOH (mM)	PVA hydroxyl:borate ratio	solution quality	dry film swelling resistance
A	1	6	21	37	precipitates	NA
B	1	2	21	111	phase separation	NA
C	1	1.2	8.4	189	stable	excellent
D	1	1.2	4.2	189	stable	excellent
E	1	0.4	4.2	567	stable	moderate
F	2	2.4	4.2	189	gels	NA
G	3	3.6	4.2	189	gels	NA

It was found that a 1% PVA-SBQ solution with a hydroxyl to borate ratio greater than ~180 produced stable solutions (examine series A through E in the table). Below a ratio of ~120 attractive forces dominated and polymers formed precipitates or phase separated solutions. Stability also decreased with increasing polymer concentration at a fixed hydroxyl to borate ratio (examine series D, F and G). This effect is likely due to an increased probability of inter-chain collision at high polymer concentrations.

Films were cast from solutions C, D and E and were photopatterned using 10 mM HCl as wet developer. Films were qualitatively judged for their ability to resist swelling upon 10 minute exposure to water. Solutions C and D gave optimal results with no evidence of swelling. Borate-modified films had the same photosensitivity as unmodified PVA-SBQ.

Thus, these studies have led to the discovery of stable PVA-SBQ/borate mixtures which yield non-swelling films that are otherwise identical in imaging properties to unaltered PVA-SBQ. This novel method of modifying PVA-SBQ is an important step in potentially developing a photoresist with enhanced photospeed suitable for high-throughput biolithography. Additional testing beyond the current study will be required to determine the ultimate utility and feasibility of PVA-SBQ/borate.

b. Polymers with Enhanced Photospeed and Dry Development

Further simplification of biolithography may be accomplished by obviating wet development entirely. We investigated this possibility by exploring the feasibility of laser-induced photoablation of dye-in-polymer composites where the dye assists in absorbing radiant laser energy of a particular wavelength [39, 40]. The wavelength is one not typically absorbed by cellular components. The biologic material is therefore translucent to the incident laser irradiation with no direct absorption of energy from the laser (contrast to excimer and CO_2 laser radiation). The energy absorbed by the dye-in-polymer composite induces an intense local thermal process (~1700 °C), resulting in rapid ablation of polymer.

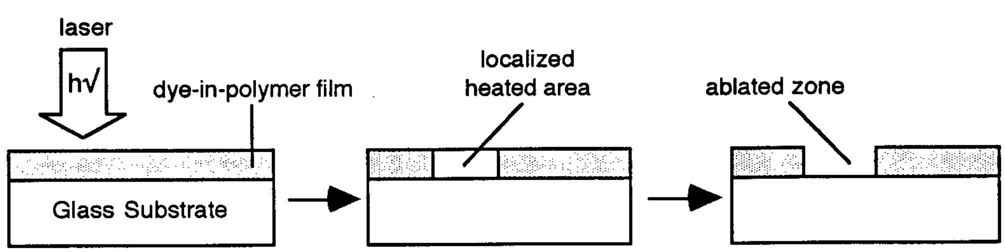

The resolution of this thermal process is governed by localized heating and thermal diffusion. It can be shown that for the thermal diffusivities of organic polymers (about 10^{-3} cm^2sec^{-1}), thermal energy conferred to the specimen will remain within the directly heated area only for very short durations (< 100 ns) [41]. This suggests that sharply-focused laser irradiation will yield high resolution images, and that the process will be biologically compatible since heating is for a very short duration, and is specific to a small volume of dye-in-polymer film.

Several dyes with high quantum yields for thermal energy conversion were tested for their ability to function as dye-in-polymer composites with poly(vinyl acetate). Dyes were selected that absorbed at wavelengths that matched those available from argon and helium-neon (He-Ne) lasers (laser use generously provided by Randy Babbitt, Department of Electrical Engineering, University of Washington). The properties of the absorbing dyes are summarized as follows:

Dye	Structure	λ_{max}	laser, λ_{ex}	solubility in 3-pentanone
Polyester yellow	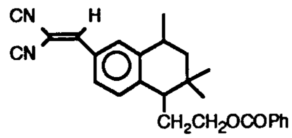	446	argon, 458	excellent
Malachite green base	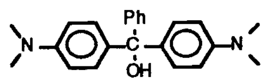	615, 425	He-Ne, 633	none
Oil nile blue	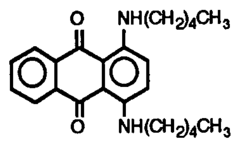	644, 596	He-Ne, 633	excellent
Solvent green 3	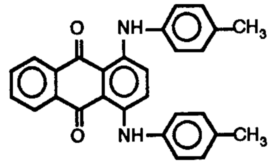	644, 607	He-Ne, 633	poor

Dyes were screened for solubility in the casting solvent 3-pentanone. Malachite green base and solvent green were both poorly soluble, and were discarded from further experiments. Polyester yellow and oil nile blue were readily soluble in 3-pentanone and formed optically clear films with poly(vinyl acetate).

Experiments were performed to determine the minimum concentration of dye required for photoablation (as a relative weight percent to polymer). Dry films (2-4 μm thick) on glass slides were prepared from solutions consisting of 10% poly(vinyl acetate) in 3-pentanone with varying concentrations of oil nile blue (0-20%). The laser write-beam was obtained from a 2 mW He-Ne laser focused with a 0.35 NA objective lens (f = 2.5 cm) to a 250 W/cm^2 spot. The focused write-beam diameter ($2w_o$) is calculated to be 30 μm according to the following equation:

$$2w_o = \left(\frac{4\lambda}{\pi}\right)\frac{f}{D}$$

where D is the diameter of the unfocused laser beam. Slides with films containing varying concentrations of dye were supported in an xyz translation stage and irradiated in the focal plane of the laser write-beam. The degree of photoablation was determined as a function of dye concentration using optical microscopy (data below):

Oil Nile Blue Concentration (%)	Degree of Photoablation
20	complete
6.6	partial
2.2	barely detectable
0.7	none
0.0	none

Thus, complete photoablation requires approximately 20% dye in the poly(vinyl acetate) film. Optical micrographs of photoablated films containing 20% oil nile blue and 20% polyester yellow are shown in FIG. 22.

Based on these encouraging results, experiments were performed to test the feasibility of isolating DNA from biologic samples using laser driven dye-in-polymer photoablation. Films containing 20% oil nile blue were formed over tonsillar tissue sections and photoablated as shown in FIG. 23. The ablated films were stable to prolonged exposure with extraction solution. However, repeated attempts to perform PCR amplification of the androgen receptor gene using this extraction solution failed to yield amplification products. Microscopic examination of post-extracted films revealed no evidence of tissue digestion in ablated regions. This suggested that failed PCR amplification was due to blockage of extraction solution by a thin layer of residual film not visible by optical microscopy.

In contrast, Law *et al.* found that irradiated films were completely removed from aluminized glass substrates in studies that examined dye-in-polymer films as potential optical recording media [39, 40]. This apparent contradiction may be due to different experimental conditions. Law *et al.* utilized very thin polymer films (0.1 μm) and very short irradiation times. They found that a 0.1 μm thick film under the action of a 8 nsec laser pulse achieves a maximum ablation contrast within 30 nsec. After this time, relaxation effects occur which result in flow of molten material back into the laser mark.

No efforts were made to control pulse duration in our experiments, and molten flow of polymer could account for the presence of a residual film. This backwards flow might also be exacerbated by our relatively thick films (40 vs. 0.1 μm). Thus, rapid dye-in-polymer biolithography may be feasible with thinner films and very short duration laser pulses. These and other experimental avenues are being actively investigated.

CONCLUSIONS

A. Result Summary

1. We report the development of a novel method termed "biolithography" which applies photolithography, a process known in the semiconductor industry, to biologic material. Biolithography utilizes a diazoquinone based photoresist and targeted light irradiation to isolate DNA from selected cell populations under direct microscopic visualization with high specificity and subcellular resolution.

2. We report the successful development of a sensitive clonality assay based on biolithography with capabilities beyond the *in situ* fluorescent assay originally proposed. The specificity for target selection is essentially 100%, and the sensitivity is at the limit of PCR.

3. Using biolithography, we have detected clonality from as few as 20 neoplastic cells and have determined that the patch size of methylation in normal females approximates macroscopic rather than microscopic dimensions.

4. We have discovered abnormal demethylation of the X chromosome at the human androgen receptor and PGK1 genes in DNA isolated from the pre-cancerous (DCIS) and invasive components of several cases of breast carcinoma.

5. Although still very preliminary, microsatellite analysis of several markers closely linked to genes involved in X chromosome inactivation has identified LOH near the XIST gene which correlates with demethylation. Consistent with the stepwise model of tumor progression, demethylation of both X chromosomes may reflect an abnormal reactivation of maternal and paternal X chromosomes.

6. Neither X chromosome demethylation or LOH could be detected using conventional microdissection methods, demonstrating the utility of biolithography to discern subtle molecular changes in solid tumors which may exist in only microscopic regions. Biolithography may thus provide new opportunities for molecular diagnostics of solid tumors.

7. Efforts have been made to increase the throughput of biolithography by exploring alternative photoresists with ultra-high photosensitivity, and laser driven systems which simplify the process steps of biolithography. Although not presently as evolved as the diazoquinone based photoresists, encouraging results have been obtained from these studies suggesting the feasibility of high-throughput biolithography.

Thus, the research has successfully addressed the Statement of Work. Superior solutions have been provided where initially proposed strategies were subsequently abandoned.

B. Implications/Recommendations

1. Clonality and Diagnostics

Clonality testing is expected to have utility for triaging patients for additional diagnostic procedures. Greater than 70% of patients samples for an abnormal mammogram have benign disease, and the majority of these would be expected to yield polyclonal results using biolithography and FNAB [3]. Patients with a polyclonal result might avoid surgical biopsy as the probability of malignancy would be very unlikely.

Our discovery of macroscopic clonal patches in normal breast increases the probability of a clonal result from benign tissue. A clonal result may therefore simply represent sampling of a normal patch rather than true neoplasia, and would require surgical biopsy for a definitive diagnosis. Fortunately, these "false positives" would be expected to represent a relatively small fraction of women undergoing screening mammography.

A potential solution to enable the use of a clonal result for tissue sections might be to identify a minimum irradiation area above which the probability of a false positive is negligible. In the case of FNAB, a minimum number of cells might be defined above which the probability of a false positive is negligible. These approaches may ultimately prove impractical however.

The finding of demethylation is presumptive evidence of carcinoma since this has not been found in normal tissues. However, the interpretation of a "negative" amplification reaction is fraught with technical difficulties related to the possibility of a failed amplification reaction. Also, the relatively low prevalence of this phenomenon makes its diagnostic usefulness unlikely.

In contrast to clonality testing, detection of mutant or deleted genetic material is generally never associated with normal tissue and may be pathognomonic of certain tumors. Defining the molecular defects in individual tumors may lead to improved diagnostics, prognostics and therapeutics. Biolithography may provide the foundation to develop routine molecular diagnostic capabilities for detecting mutations and deletions in breast carcinoma.

2. Translational Development

A number of avenues may be pursued to expand the throughput and other capabilities of biolithography so that it may directly benefit patients in a clinical laboratory. With further development, biolithography should provide new opportunities to perform molecular diagnostics on breast cancer and other solid tumors. Presently, biolithography is a manual and labor intensive method appropriate for the research laboratory. Translation to the clinical laboratory could be promoted by the development of automation and novel photoresist materials with increased photospeed.

3. Demethylation and Basic Mechanisms of Carcinogenesis

The surprising finding of demethylation of the X chromosomes in breast cancer and its precursor lesions should be further explored. This finding opens up a host of new questions regarding the control of X inactivation and carcinogenesis. What is the mechanism of methylation and demethylation? Does demethylation result in net activation or inactivation of the X chromosomes? Is it related to disruption of components within the XIC.

Such questions might be further clarified by experiments to determine if there is biallelic expression of X-linked genes and XIST in particular. Unfortunately, isolation of RNA from paraffin sections using biolithography has not yet been successful. The microsattelite analysis should be expanded to determine if there is a statistically significant correlation between LOH and demethylation. If so, then experiments would need to determine whether the markers are deleted from the active or inactive X chromosome.

REFERENCES

1. Miller, B.A., E.J. Feuer, and B.F. Hankey, Recent incidence trends for breast cancer in women and relevance of early detection: An update. CA Cancer Journal for Clinicians, 1993. **43**(1): p. 27-41.
2. Strax, P., Detection of breast cancer. Cancer, 1990. **66**(Suppl): p. 1336-1340.
3. Sickles, E.A., Quality Assurance. Radiologic Clinics of North America, 1992. **30**(1): p. 265-275.
4. Cyrlak, D., Induced costs of low-cost screening mammography. Radiology, 1988. **168**: p. 661-663.
5. Jackson, V.P., The status of mammographically guided fine needle aspiration biopsy of nonpalpable breast lesions. Radiologic Clinics of North America, 1992. **30**(1): p. 155-166.
6. Layfield, L., Can fine-needle aspiration replace open biopsy in the diagnosis of palpable breast lesions. American Journal of Clinical Pathology, 1992. **98**: p. 145-147.
7. Layfield, L., E. Chrischilles, M. Cohen, and K. Bottles, The palpable breast nodule: a cost-effectiveness analysis of alternate diagnostic approaches. Cancer, 1993. **72**: p. 1642-1651.
8. Orell, S.R., G.F. Sterrett, M.N.-I. Walters, and D. Whitaker, Manual and Atlas of Fine Needle Aspiration Cytology. 2nd editon ed. 1992, New York: Churchill Livingstone Inc. 341.
9. Noguchi, S., K. Motomura, H. Inaji, S. Imaoka, and H. Koyama, Clonal analysis of fibroadenoma and phyllodes tumor of the breast. Cancer Res, 1993. **53**: p. 4071-4074.
10. Allen, R.C., H.Y. Zoghbi, A.B. Moseley, H.M. Rosenblatt, and J.W. Belmont, Methylation of *Hpa*II and *Hha*I sites near the polymorphic CAG repeat in the human androgen-receptor gene correlates with X chromosome inactivation. Am J Hum Genet, 1992. **51**: p. 1229-1239.
11. Noguchi, S., K. Motomura, H. Inaji, S. Imaoka, and H. Koyama, Clonal analysis of predominantly intraductal carcinoma and precancerous lesions of the breast by means of the polymerase chain reaction. Cancer Res, 1994. **54**: p. 1849-1853.
12. Fearon, E.R., S.R. Hamilton, and B. Vogelstein, Clonal analysis of human colorectal tumors. Science, 1987. **238**: p. 193-7.
13. Radford, D.M., *et al.*, Allelic loss on a chromosome 17 in ductal carcinoma in situ of the breast. Cancer Res., 1993. **53**: p. 2947-9.
14. Kovach, J.S., R.M. McGovern, J.D. Cassady, S.K. Swanson, L.E. Wold, B. Vogelstein, and S.S. Sommer, Direct sequencing from touch preparations of human carcinomas: analysis of p53 mutations in breast carcinomas. J. Natl. Cancer Inst, 1991. **83**: p. 1004-9.
15. Emmert-Buck, M.R., *et al.*, Increased gelatinase A (MMP-2) and cathespin B activity in invasive tumor regions of human colon cancer samples. Am. J. Pathol., 1994. **145**: p. 1285-90.
16. Zhuang, Z., P. Bertheau, M.R. Emmert-Buck, L.A. Liotta, J. Gnarra, W.M. Linehan, and I.A. Lubensky, A microdissection technique for archival DNA analysis of specific cell populations in lesions <1mm in size. Am. J. Pathol., 1995. **146**: p. 620-5.

17. Caldas, C., *et al.*, Frequent somatic mutation and homozygous deletions of the p16 (MTS1) gene in pancreatic adenocarcinoma. Nature Genet., 1994. **8**: p. 27-32.
18. Schutte, M., *et al.*, Identification by representational difference analysis of a homozygous deletion in pancreatic carcinoma that lies within the BRCA2 region. Proc. Natl. Acad. Sci. USA, 1995. **92**: p. 5950-4.
19. Shibata, D., D. Hawes, Z.H. Li, A.M. Hernandez, C.H. Spruck, and P.W. Nichols, Specific genetic analysis of microscopic tissue after selective ultraviolet radiation fractionation and the polymerase chain reaction. Am. J. Pathol., 1992. **141**: p. 539-43.
20. Emmert-Buck, M.R., *et al.*, Laser capture microdissection. Science, 1996. **274**: p. 998-1001.
21. DeForest, Photoresist Materials and Processes. 1975, McGraw-Hill.
22. Pacansky and Lyerta, Photochemical decomposition mechanisms for AZ-type photoresists. IBM J. Res. Dev., 1979. **23**(1): p. 42.
23. Lyon, M.F., X-chromosome inactivation and developmental patterns in mammals. Biol Rev, 1972. **47**: p. 1-35.
24. Fialkow, P.J., Clonal origin of human tumors. Biochim Biophys Acta, 1976. **458**: p. 283-321.
25. Knudson, A.G., Hereditary cancer, oncogenes, and antioncogenes. Cancer Res, 1985. **45**: p. 1437-1443.
26. Noguchi, S., K. Motomura, H. Inaji, S. Imaoka, and H. Koyama, Clonal analysis of human breast cancer by means of the polymerase chain reaction. Cancer Res, 1992. **52**: p. 6594-6597.
27. Tsai, Y.C., Y. Lu, P.W. Nichols, G. Zlotnikov, P.A. Jones, and H.S. Smith, Contiguous patches of normal human mammary epithelium derived from a single stem cell: Implications for breast carcinogenesis. Cancer Res, 1996. **56**: p. 402-4.
28. Feinberg, A.P. and B. Vogelstein, Hypomethylation distinguishes genes of some human cancers from their normal counterparts. Nature, 1983. **301**: p. 89-92.
29. Feinberg, A.P., Genomic imprinting and gene activation in cancer. Nature Genetics, 1993. **4**: p. 110-113.
30. Rainier, S., L.A. Johnson, C.J. Dobry, A.J. Ping, P.E. Grundy, and A.P. Feinberg, Relaxation of imprinted genes in human cancer. Nature, 1993. **362**: p. 747-749.
31. Panning, B. and R. Jaenisch, DNA hypomethylation can activate Xist expression and silence X-linked genes. Gen Dev., 1996. **10**: p. 1991-2002.
32. Lyon, M.F., Pinpointing the centre. Nature, 1996. **379**: p. 116-117.
33. Willard, H.F., X chromosome inactivation, XIST, and pursuit of the X-inactivation center. Cell, 1996. **86**: p. 5-7.
34. Heard, E. and P. Avner, Role play in X-inactivation. Human Mol. Genet., 1994. **3**: p. 1481-1485.
35. Penny, G.D., G.F. Kay, S.A. Sheardown, S. Rastan, and N. Brockdorff, Requirement for Xist in X chromosome inactivation. Nature, 1996. **379**: p. 131-137.
36. Brown, C.J. and H.F. Willard, The human X-inactivation centre is not required for maintenance of X-chromosome inactivation. Nature, 1994. **368**: p. 154-156.
37. Ichimura, K., Photocrosslinkable poly(vinyl alcohols): Preparation, properties and applications. Heterogeneous Chemistry Reviews, 1996. **3**: p. 419-441.

38. Kurokawa, H., M. Shibayama, T. Ishimaru, and S. Nomura, Phase behaviour and sol-gel transition of poly(vinyl alcohol) - borate complex in aqueous solution. Polymer, 1992. **33**(10): p. 2182-88.
39. Law, K.Y., Ablative optical recording using organic dye-in-polymer thin films: Some mechanistic aspects. J. Appl. Phys., 1983. **54**(9): p. 4799-4805.
40. Law, K.Y. and P.S. Vincett, Dye-in-polymer films for ablative optical recording with GaAs diode lasers. Appl. Phys. Lett., 1981. **39**(9): p. 718-20.
41. Sonnenschein, M.F., A.M. Kotliar, and C.M. Roland, Poly(ethylene terphthalate) crystallization as a method for microlithography. Polymer Engineering and Science, 1990. **30**(18): p. 1165-70.

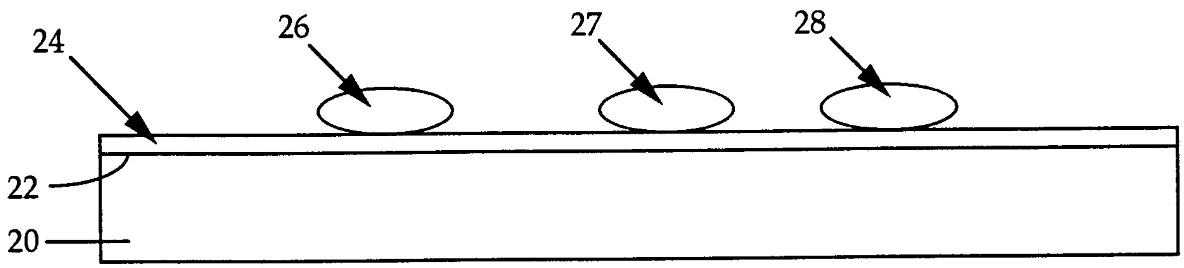

FIG. 1

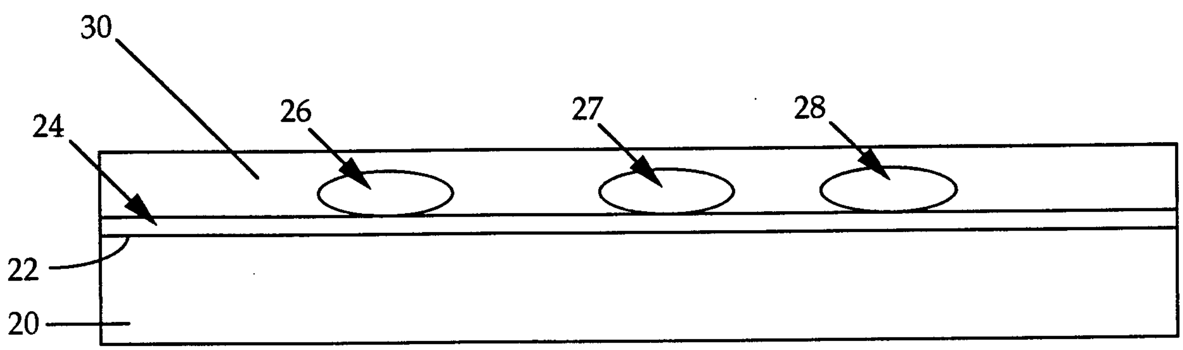

FIG. 2

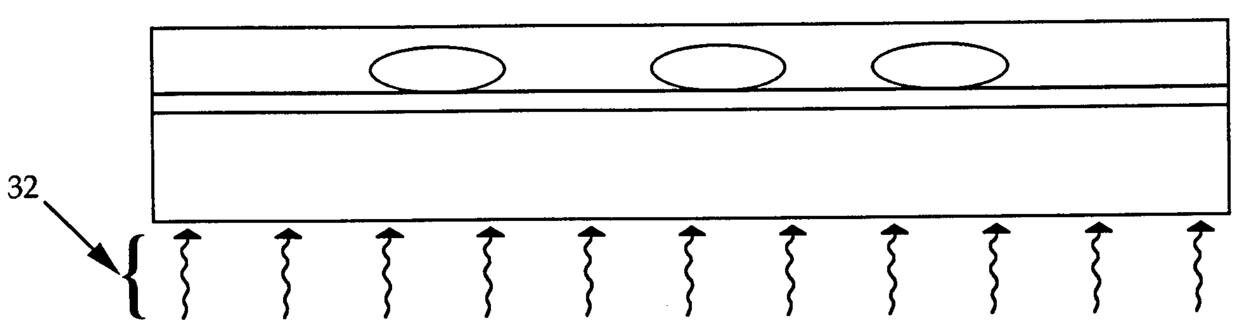

FIG. 3

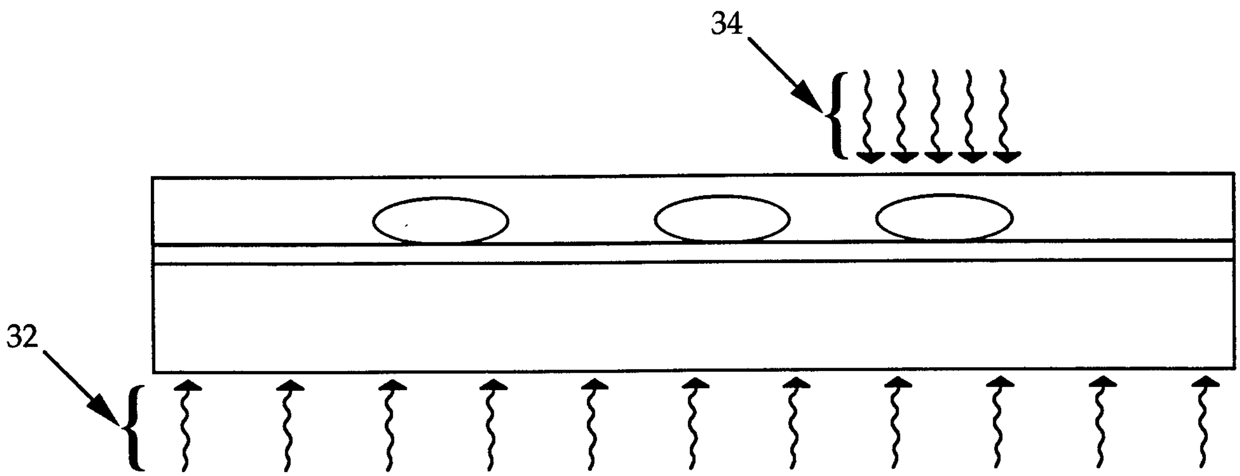

FIG. 4

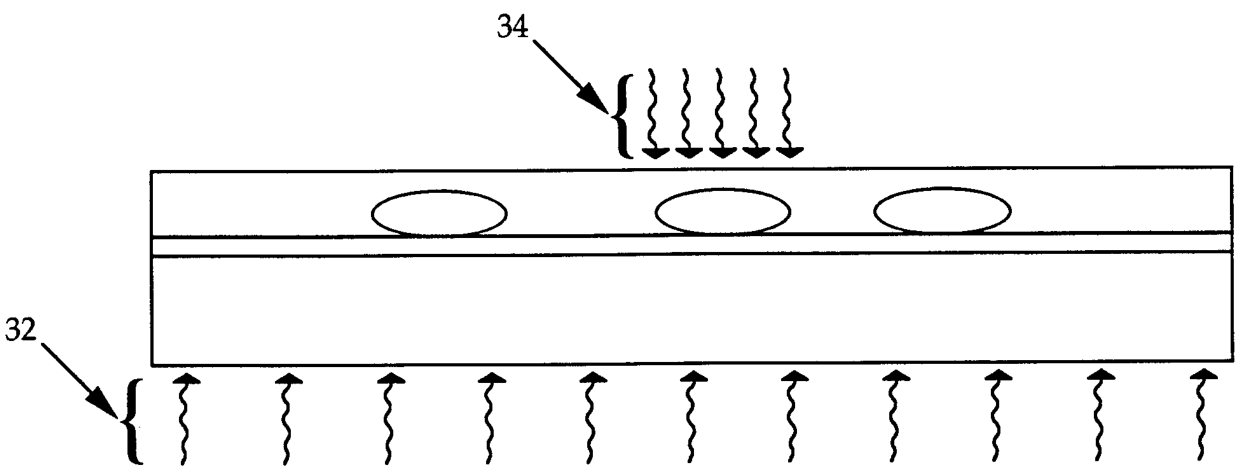

FIG. 5

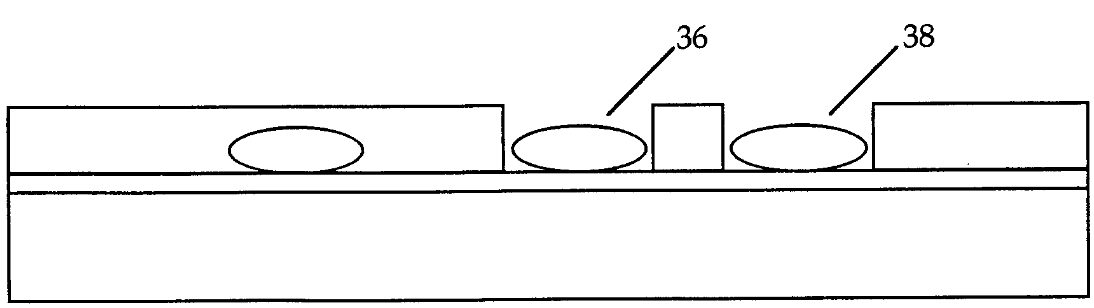

FIG. 6

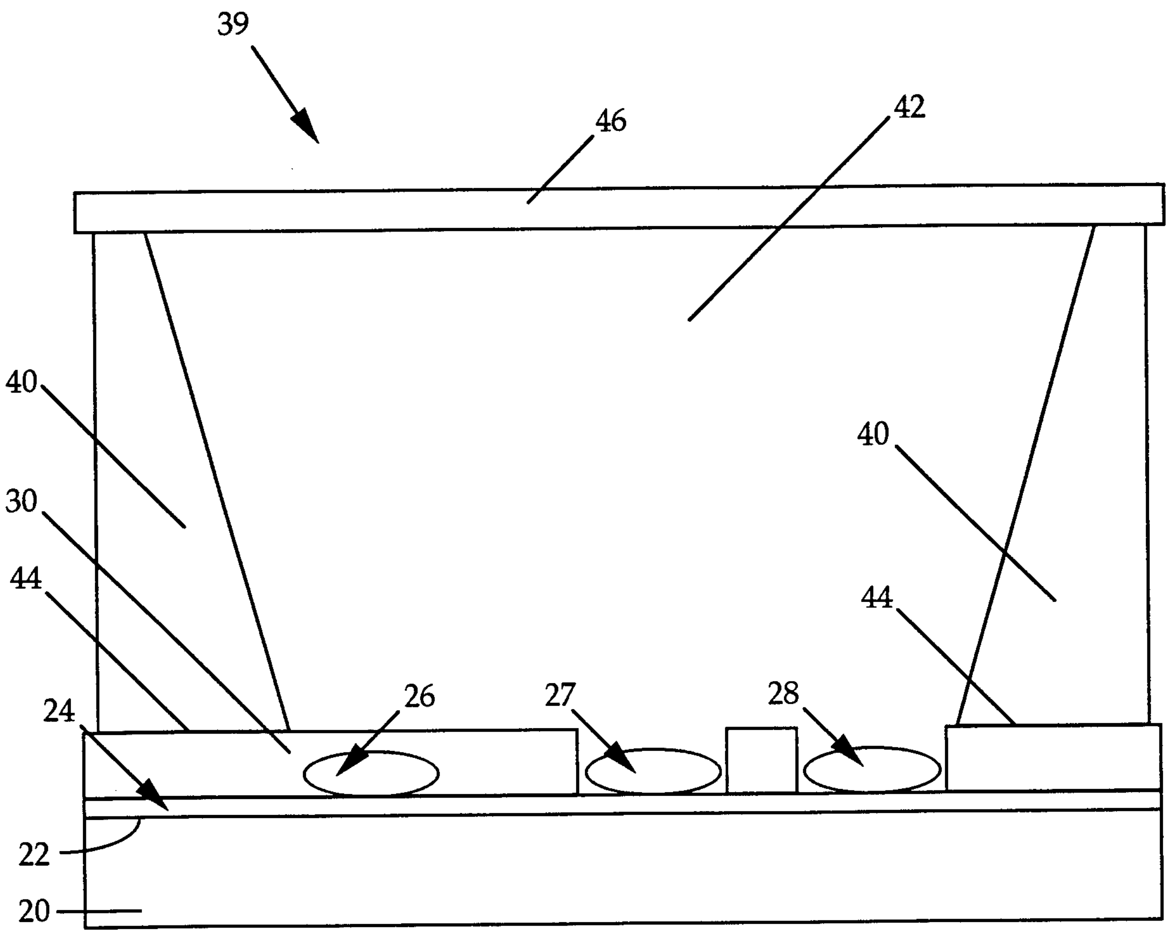

FIG. 7

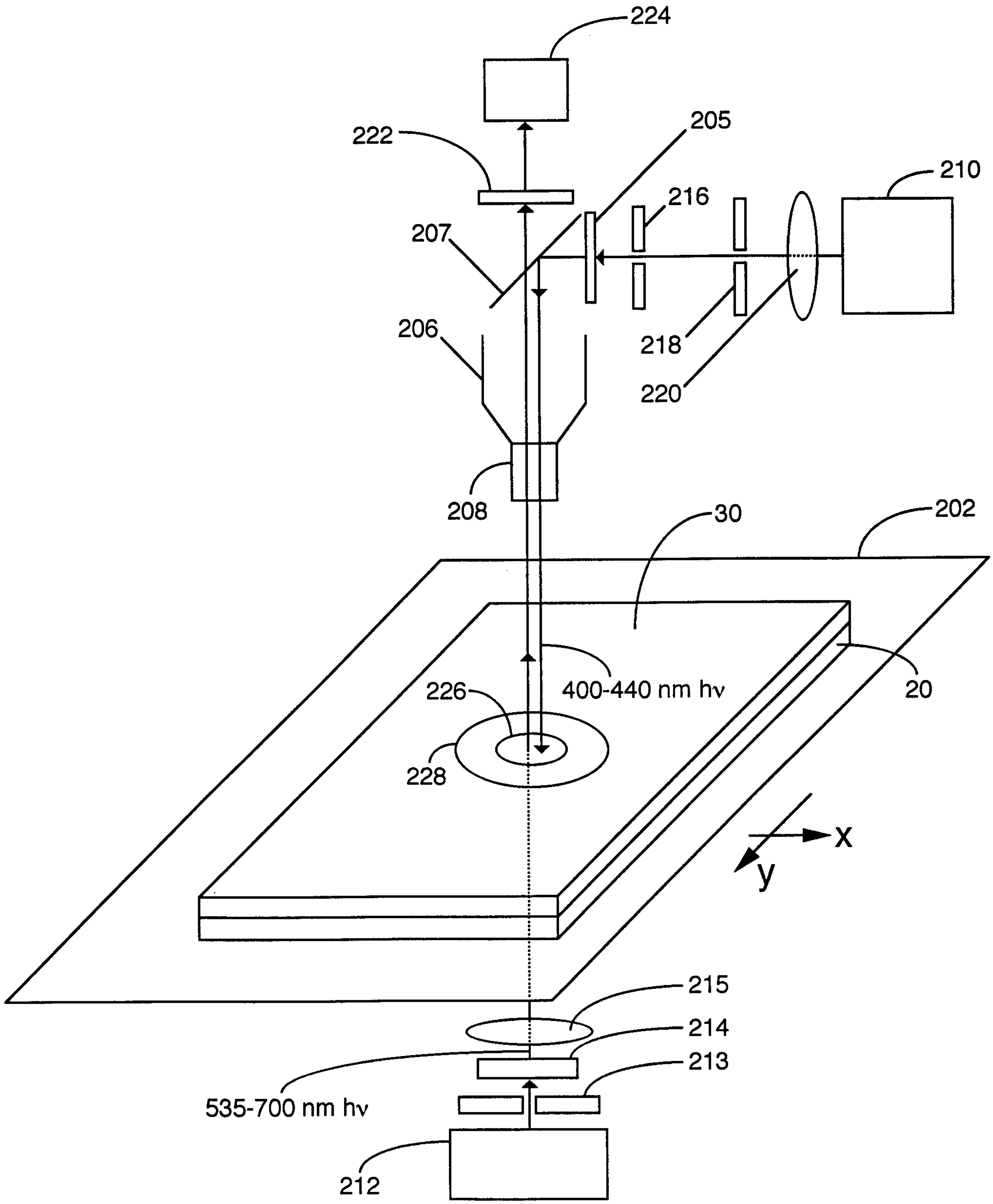
224
222
205
210
216
207
206
218
220
208
30
202
226
400-440 nm hν
20
228
x
y
215
214
213
535-700 nm hν
212

FIG. 8

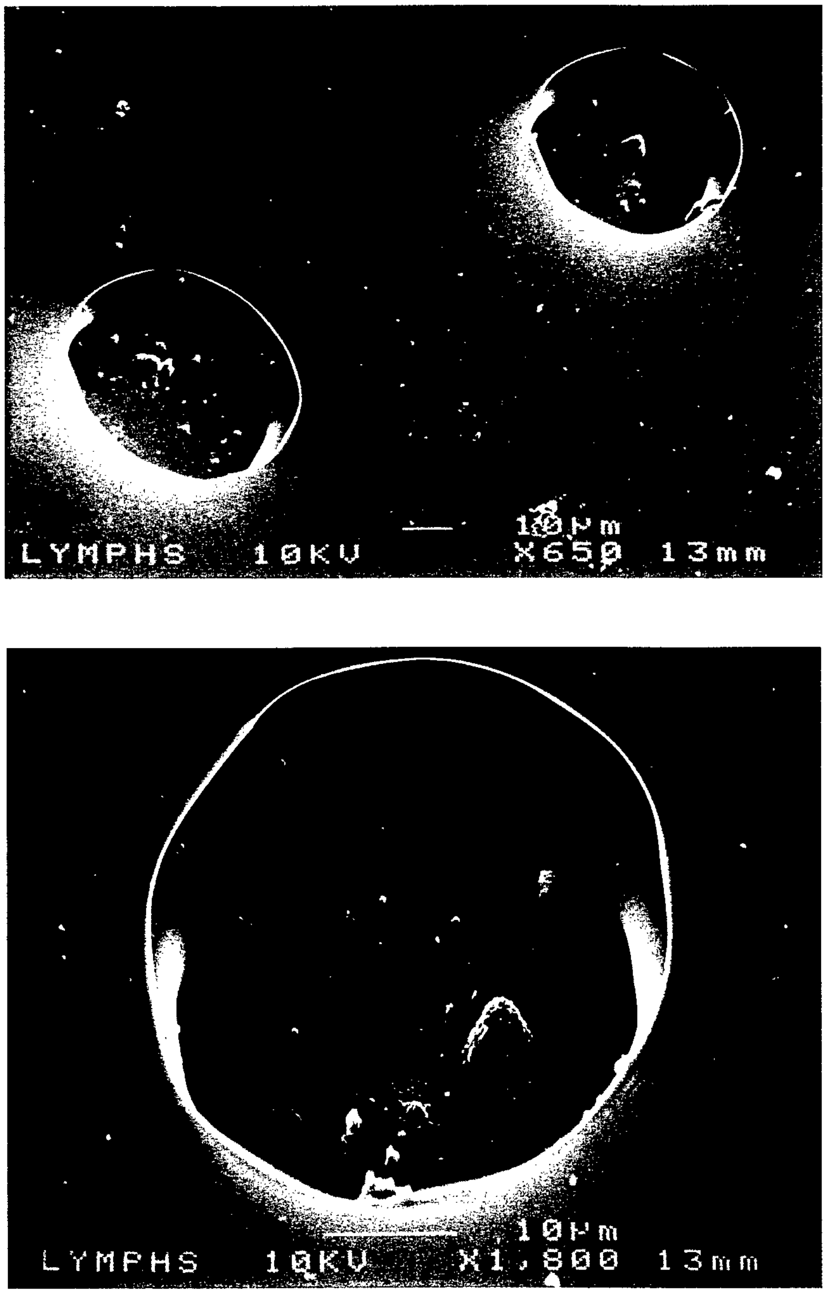

FIG. 9

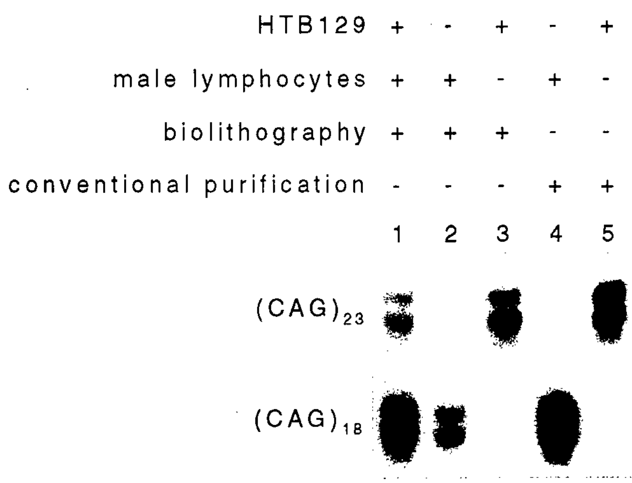

FIG. 10

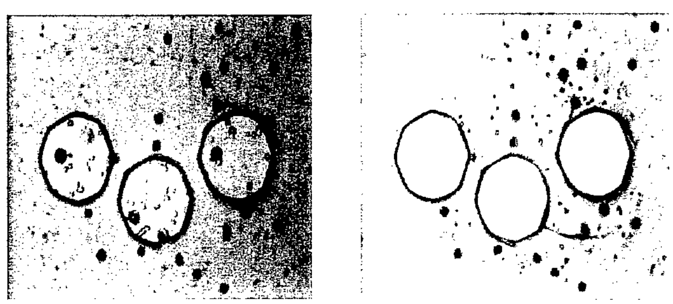

Before protease After protease

FIG. 11

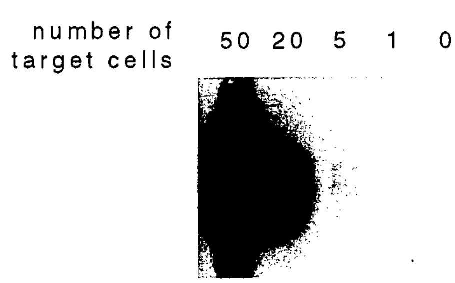

FIG. 12

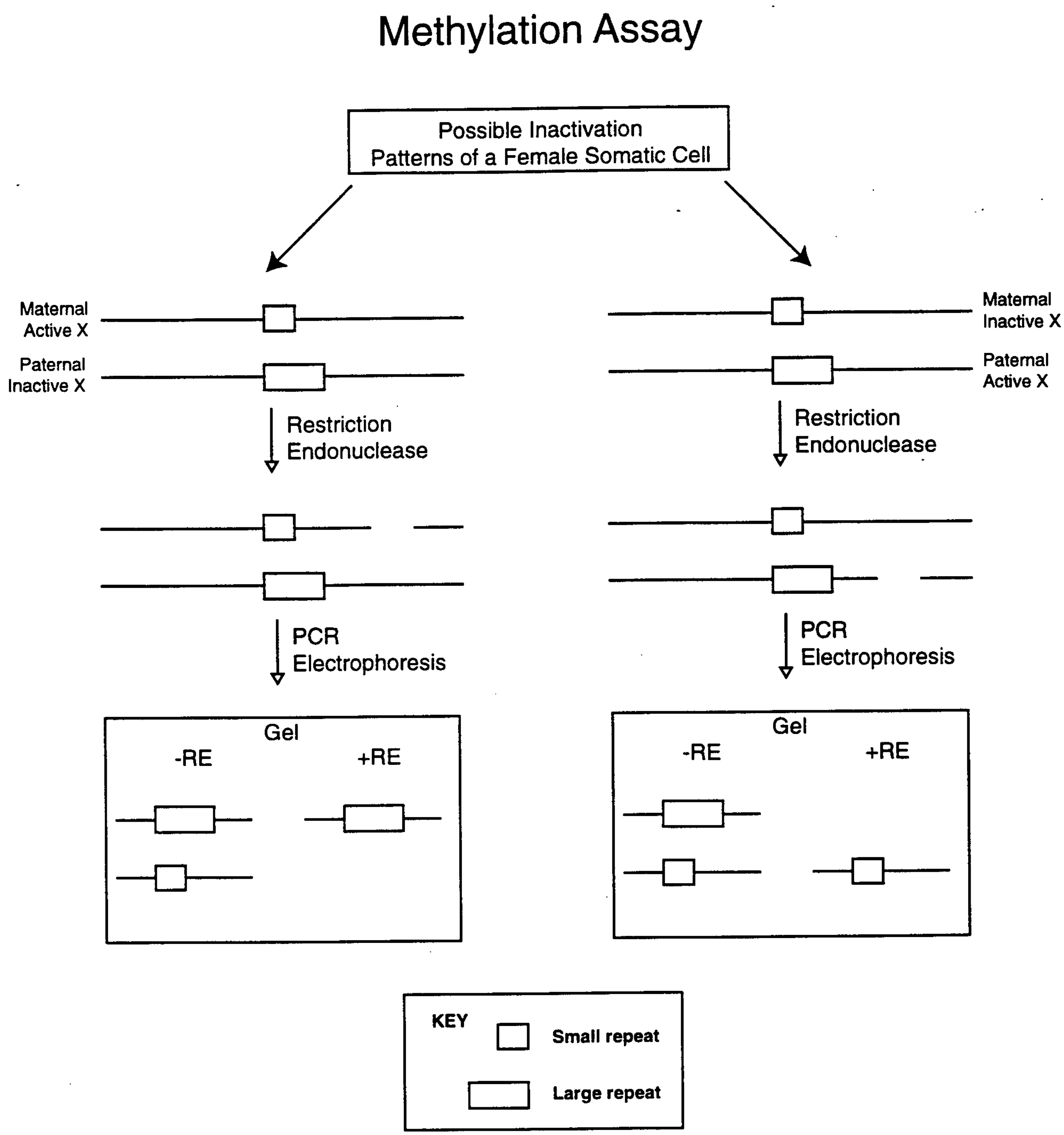

Methylation Assay
Possible Inactivation Patterns of a Female Somatic Cell
Maternal Active X
Paternal Inactive X
Maternal Inactive X
Paternal Active X
Restriction Endonuclease
Restriction Endonuclease
PCR Electrophoresis
PCR Electrophoresis
Gel
-RE
+RE
Gel
-RE
+RE
KEY
Small repeat
Large repeat

FIG. 13

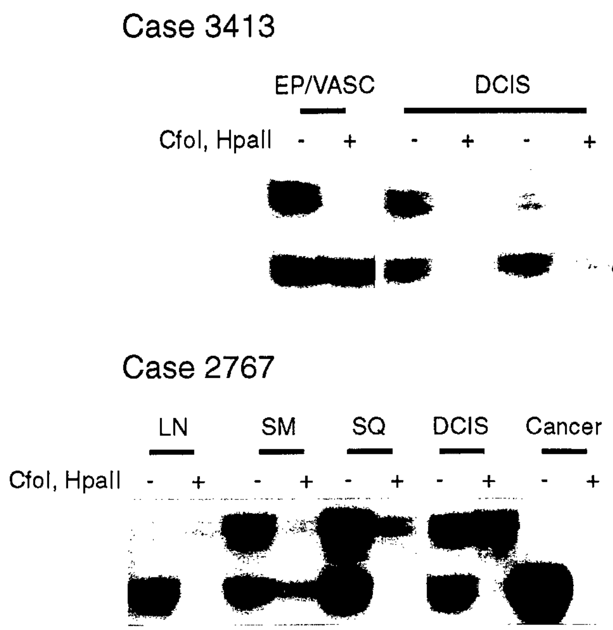
Case 3413
EP/VASC
DCIS
Cfol, Hpall - + - + - +
Case 2767
LN
SM
SQ
DCIS
Cancer
Cfol, Hpall - + - + - + - + - +

FIG. 14

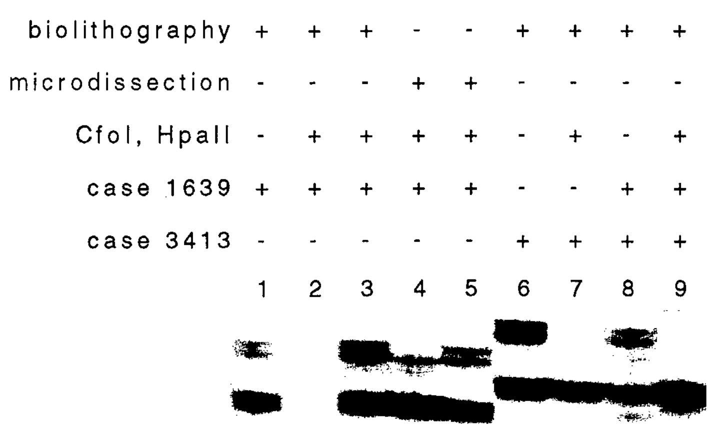
biolithography + + + - - + + + +
microdissection - - - + + - - - -
Cfol, Hpall - + + + + - + - +
case 1639 + + + + + - - + +
case 3413 - - - - - + + + +
1 2 3 4 5 6 7 8 9

FIG. 15

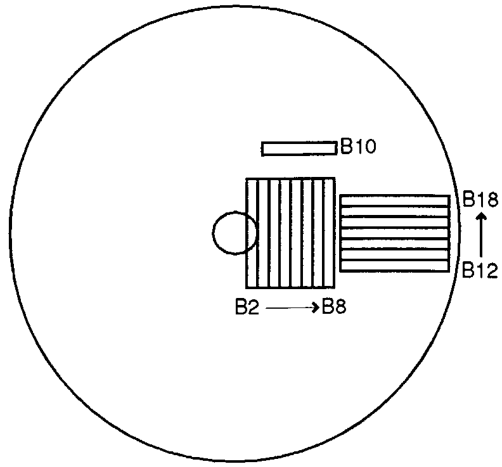

Case 1196
androgen receptor gene

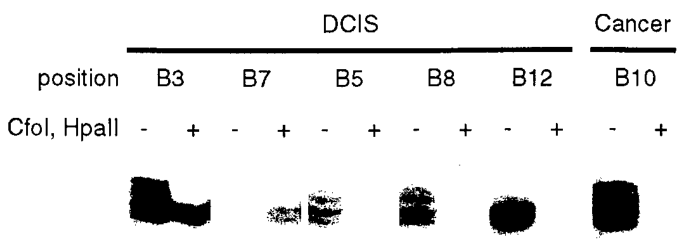

FIG. 16a

Case 1196
PGK1 gene

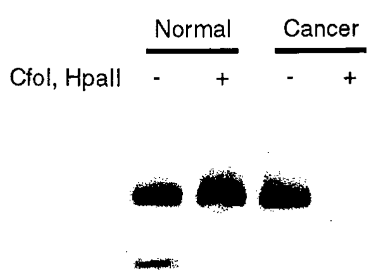

FIG. 16b

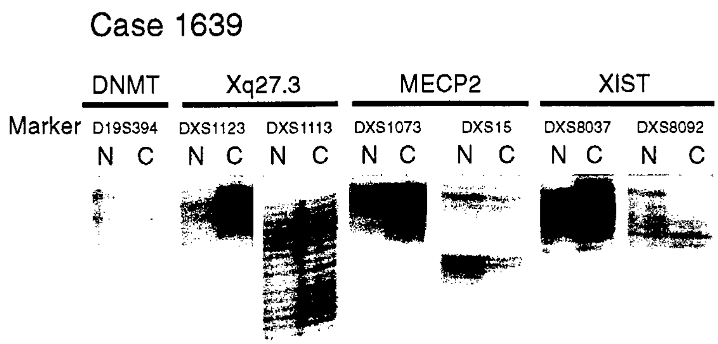

FIG. 17

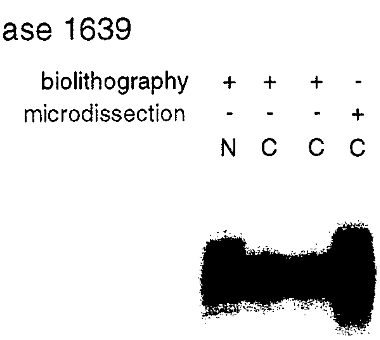

FIG. 18

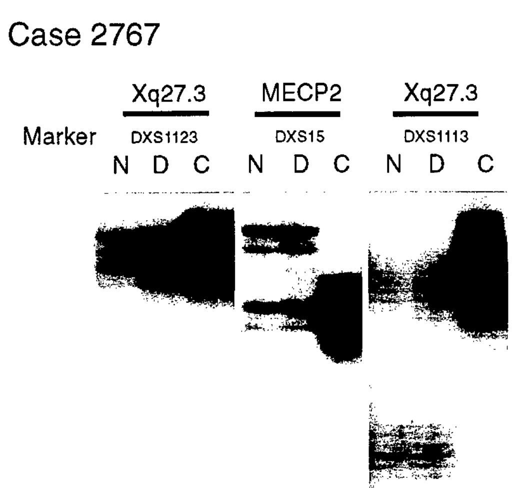

FIG. 19

FIG. 20

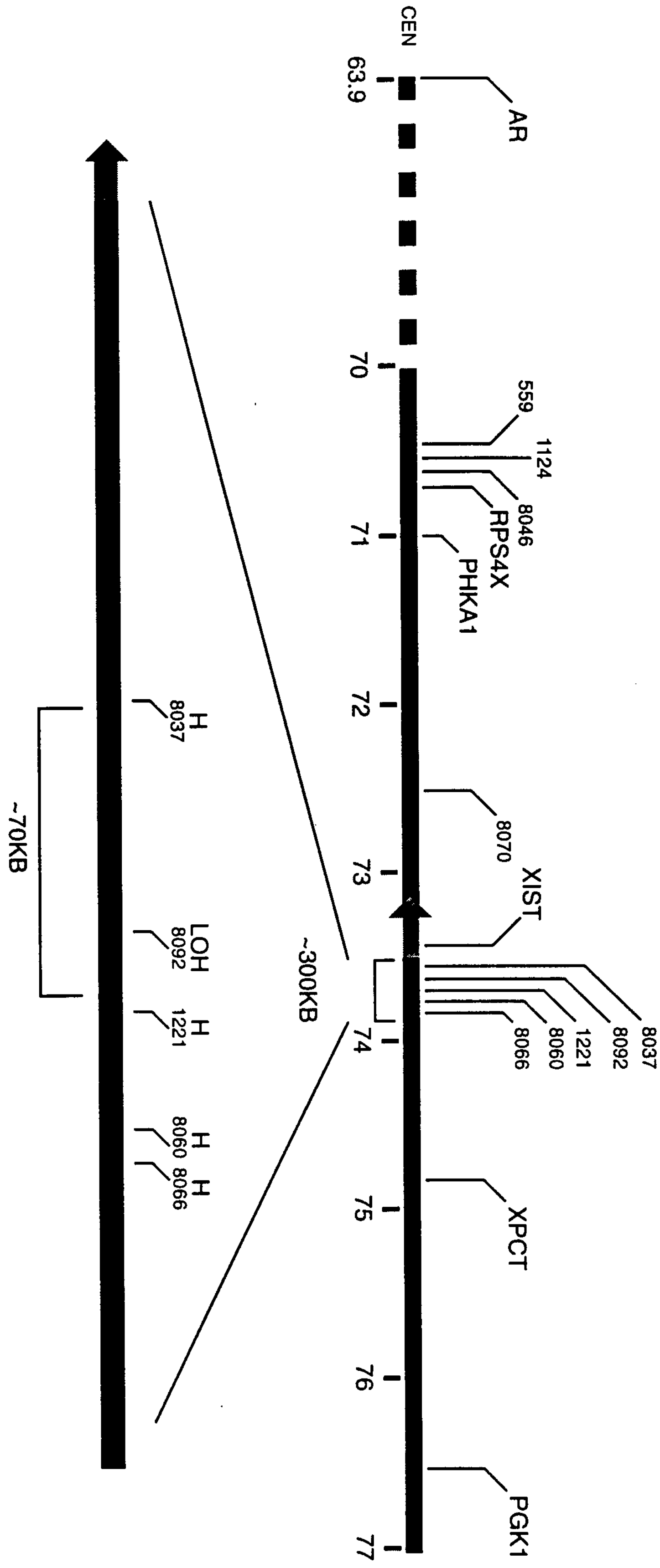

CEN
63.9
AR
70
559
1124
8046
RPS4X
71
PHKA1
72
8070
73
XIST
8037
8092
1221
8060
8066
74
75
XPCT
76
PGK1
77
~300KB
H
8037
LOH
8092
H
1221
H
8060
H
8066
~70KB

FIG. 21

Demethylation Model of the X chromosome in breast carcinogenesis

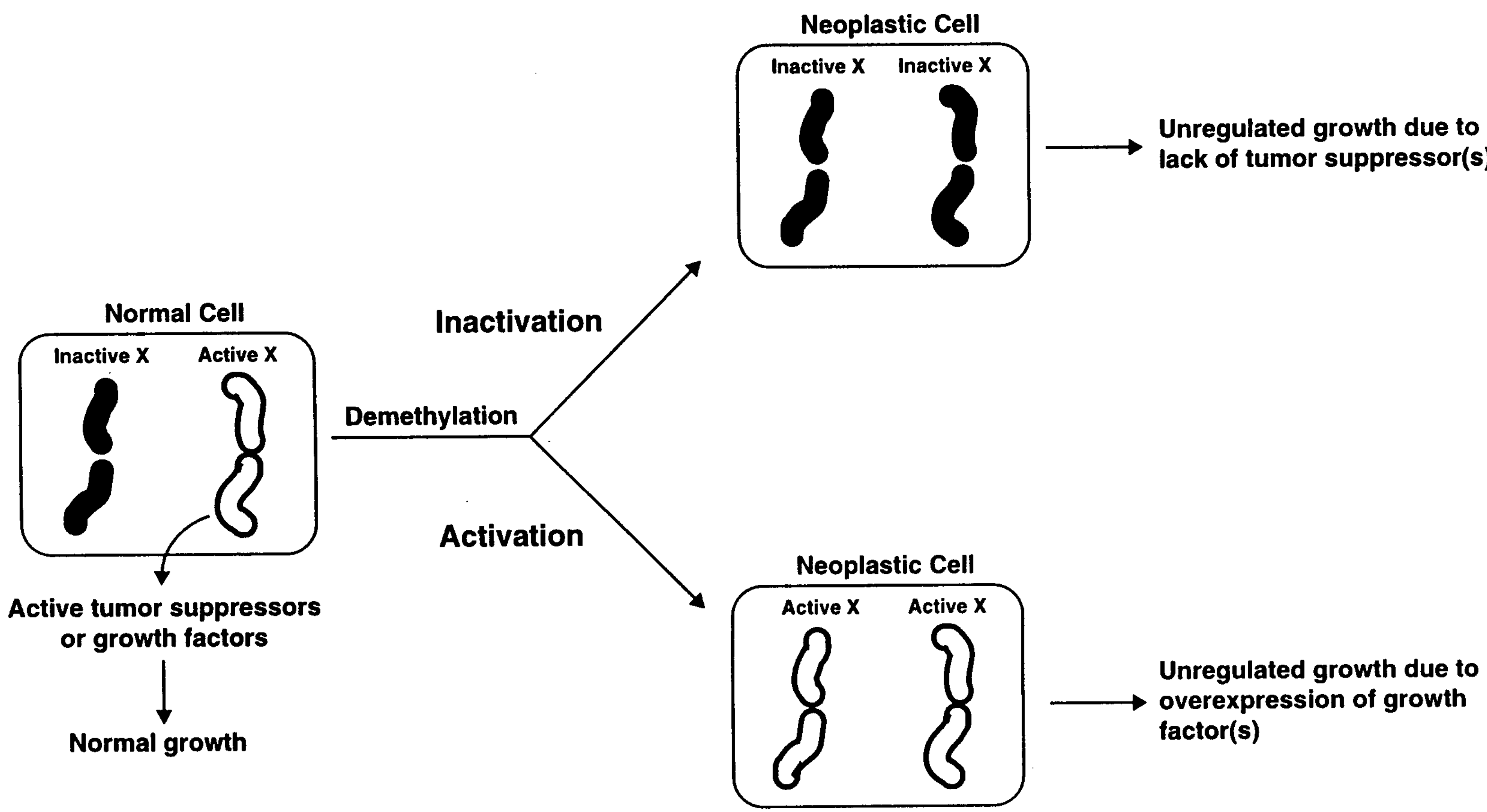

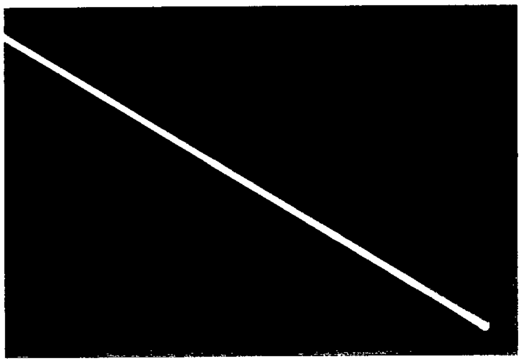

Oil Nile Blue

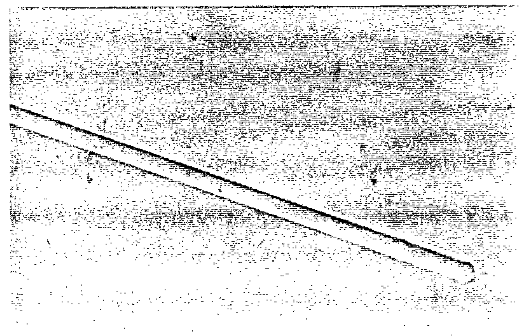

Polyester Yellow

FIG. 22

FIG. 23

Table I

Case	glandular epithelium	squamous epithelium	smooth muscle	lymph node	DCIS	invasive cancer	metastatic cancer
1196	3M1	M1	M1	-	2M1, 4M0	M0	-
1639	-	M2	-	-	M0	2M0	-
2767	-	M1	M2	M1	M1	deletion	-
1659	-	-	-	-	M1	-	-
3413	M1	-	-	-	3M1	-	-
3839	-	M1	-	M2	2M1, 2M0	-	M1
1049	-	-	-	-	M1	-	-

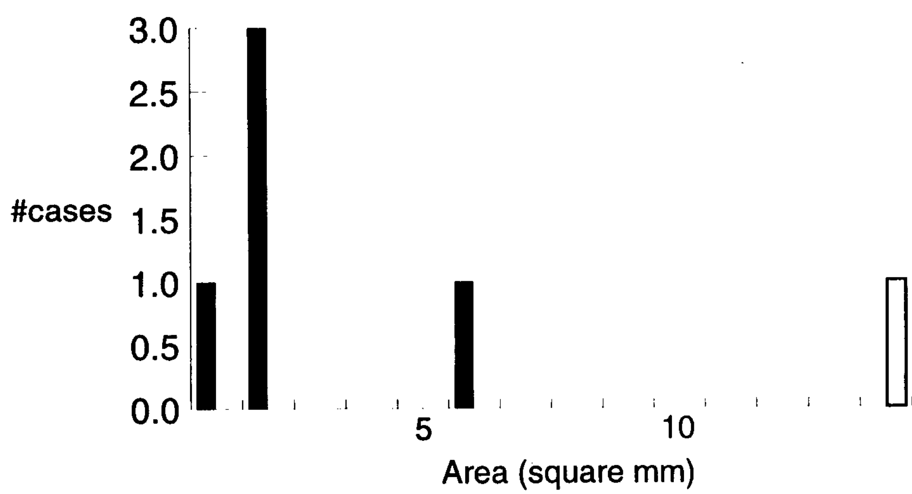

Table II

Locus		Xq27-Xq28					MECP2		XIST								DNMT			
Position (MB)		(150.99-153.10)					(158.20)		(73.42)								(14.05)			
microsatellite		1215	8091	1193	1123	1113	15	1073	8066	1221	8092	8037	8070	8046	1124	559	413	394	584	221
position (MB)		151.9	152.0	153.0	153.0	153.2	157.2	158.5	73.66	73.62	73.60	73.55	72.50	70.62	70.57	70.52	12.20	14.10	14.85	15.60
heterozygosity		.55	.76	.75	.68	.75	.84	-	.77	.59	.87	.74	.45	.49	.55	.74	.78	.92	.40	.87
case	methylation																			
1196																				
native x 8	+	H	H	H	H	H	H	H	H	H	**N**	**N**	**N**	H	H	H	H	H	H	H
dcis x 7	+/-	H			H	H	H	H	H	H	**N**	**N**	**N**	H	H	H	H	H		
cancer	-	H	H	H	H	H	H	H	H	H	**N**	**N**	**N**	H	H	H	H	H	H	H
1639																				
native	+				H	H	H	H	H	H	**H**	H	H	H	H	N		H		
cancer x 3	-				H	H	H	H	H	H	**LOH**	H	H	H	H	N		H		
3839																				
native	+	N			H	H	H	N	H	N	H	N	H	H		H		H		
dcis x 4	+/-	N			H	H	H	N	H	N	H	N	H	H		H		H		
cancer	+	N			H	H	H	N	H	N	H	N	H	H		H		H		
2767																				
native	+	N			H	H	H	N	H	N	H	N	N	H		N		H		
dcis	+	N			H	H	H	N	H	N	H	N	N	H		N		H		
cancer	?	N			H	**LOH**	**LOH**	N	H	N	H	N	N	H		N		H		
1659																				
dcis	+										H									
1049																				
dcis	+										N									
3413																				
dcis	+										H									

Bibliography

Recipients of Salary: John A. Zebala, M.D., Ph.D.

Venues of Presentation:

Work presented in detail in an oral presentation and also in abstract at the meeting of the Academy of Clinical Laboratory Physicians and Scientists in Minneapolis, Minnesota on June 5-7, 1997. Other manuscripts describing the work are in preparation.